AD-A188 818 COMPRESSIBLE FRICTION COEFFICIENTS IN A SIMULATED HEAT PIPE(U) AIR FORCE INST OF TECH WRIGHT-PATTERSON AFB OH SCHOOL OF ENGIEERING C A HOLLADAY DEC 87 1/1

UNCLASSIFIED AFIT/GAE/AA/87D-6 F/G 13/1 NL

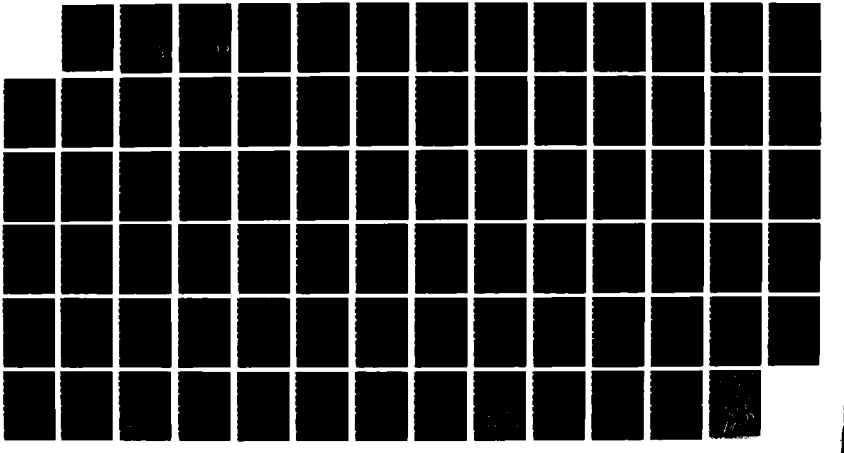

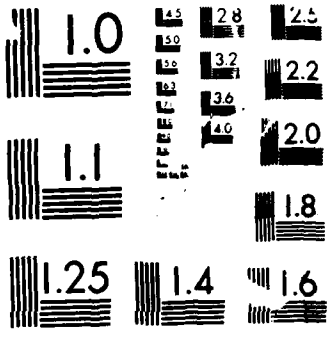

MICROCOPY RESOLUTION TEST CHART
DS-1963-A

DTIC FILE COPY

AD-A188 818

COMPRESSIBLE FRICTION COEFFICIENTS IN A SIMULATED HEAT PIPE

THESIS

Constance A. Holladay
Second Lieutenant, USAF

AFIT/GAE/AA/87D-6

DTIC
ELECTE
FEB 0 8 1988
S
H

DEPARTMENT OF THE AIR FORCE
AIR UNIVERSITY
AIR FORCE INSTITUTE OF TECHNOLOGY

Wright-Patterson Air Force Base, Ohio

DISTRIBUTION STATEMENT A
Approved for public release;
Distribution Unlimited

88 2 02 061

AFIT/GAE/AA/87D-6

COMPRESSIBLE FRICTION COEFFICIENTS IN A SIMULATED HEAT PIPE

THESIS

Constance A. Holladay
Second Lieutenant, USAF

AFIT/GAE/AA/87D-6

DTIC
ELECTE
FEB 08 1988
S D
H

Approved for public release; distribution unlimited

AFIT/GAE/AA/87D-6

COMPRESSIBLE FRICTION COEFFICIENTS IN A SIMULATED HEAT PIPE

THESIS

Presented to the Faculty of the School of Engineering
of the Air Force Institute of Technology
Air University
In Partial Fulfillment of the
Requirements for the Degree of
Master of Science in Aeronautical Engineering

DTIC COPY INSPECTED

Constance A. Holladay, B.S.
Second Lieutenant, USAF

December 1987

Accession For
NTIS GRA&I ☑
DTIC TAB ☐
Unannounced ☐
Justification
By
Distribution/
Availability Codes
Dist | Avail and/or Special
A-1

Approved for public release; distribution unlimited.

Acknowledgements

Throughout the work on this thesis I have received a great deal of help and support from several people. I am deeply indebted to my faculty advisor, Dr. James Hitchcock, for the invaluable guidance and assistance he provided throughout my research. Without his help, this thesis might not have been completed. In any experimental research, problems with the equipment will inevitably arise. I would like to thank all of the technicians in the Aeronautics/Astronautics laboratories at AFIT, especially Leroy Cannon, for their help on the numerous occasions when problems with my equipment came up. Finally, I wish to thank my fiance Mike for his continual support and encouragement during my entire thesis work.

Constance A. Holladay

Table of Contents

	Page
Acknowledgements	ii
List of Figures	v
List of Symbols	vi
Abstract	viii
I. Introduction	1
Development and Operation of the Heat Pipe	1
Background Literature	4
Objective and Scope	7
II. Experimental Model	8
Heat Pipe Simulation	8
Experimental Apparatus	9
Pipe Calibration	12
Data Measurement and Acquisition	13
Experimental Results	18
III. Numerical Model	21
Governing Equations	21
Incompressible Model	21
Compressible Model	25
Solution Method	27
Numerical Results	28
IV. Discussion of Results	31
Experimental Results Discussion	31
Numerical Results Discussion	34
V. Conclusions and Recommendations	38
Conclusions	38
Recommendations	39
Appendix A: Raw Experimental Pressure Data	41
Appendix B: Sample Calculations	47

Appendix C: Numerical Simulation Code and Sample Results 53

Bibliography 66

Vita 67

List fo Figures

Figure		Page
1.1	Diagram of the Thermal Syphon	3
1.2	Components and Operation of a Conventional Heat Pipe (3:2)	3
1.3	Development of Capillary Pressure at the Liquid Vapor Interface (3:2)	4
2.1	Experimental Test Configuration	11
2.2	Porous Pipe Calibration Manifold (Bowman 2:29).	12
2.3	Porous Pipe Calibration Data Showing Offset From Origin	14
2.4	Porous Pipe Calibration Results	15
2.5	Enlargement of (Δp^2) Range of 0 - 500,000 lbf^2/ft^4 in Calibration Results	16
2.6	Axial Pressure Distributions	20
3.1	Element of Fluid for Equation of Motion	21
3.2	Element of Fluid Used for Mass Balance	23
3.3	Pressure Interpolation	24
3.4	Force Balance on Entire Heat Pipe	28
3.5	Effect of Compressibility in Evaporator	29
3.6	Effect of Compressibility in Condenser	30
B.1	Calibration Manifold	47

List of Symbols

a - speed of sound in air (ft/sec)

A_{cs} - porous pipe cross-sectional area (ft^2)

A_s - porous pipe surface area (ft^2)

A - constant used in equation 2.1 (ft^2/sec^2)

B - constant used in equation 2.1 (lbf/ft-sec)

C - discharge coefficient

D - porous pipe inside diameter (ft)

d - orifice plate bore (ft)

f - friction coefficient

F_e - thermal expansion factor

g_c - constant in Newton's second law

k - ratio of specific heats

L - length (ft)

m - mass (lbm)

$\dot{m}$ - mass flow rate (lbm/sec)

M - rate of flow momentum ($lbm\text{-}ft/sec^2$)

Ma - Mach number

p - pressure (lbf/ft^2)

PL - total length of simulated heat pipe (ft)

R - ideal gas constant for air ($lbf\text{-}ft/lbm/^\circ R$)

Re_x - axial Reynolds number

Re_y - radial Reynolds number

T - temperature ($^\circ R$)

u - axial velocity (ft/sec)

v - radial velocity (ft/sec)

x - axial location along porous pipe (ft)

Y - compressibility expansion factor

β_a - ratio of diameters (d/D)

ρ - density (lbm/ft^3)

τ_w - wall shear stress (lbf/ft^2)

μ - viscosity ($lbf\text{-}sec/ft^2$)

Subscripts

1 - upstream end of Δx increment

2 - downstream end of Δx increment

Abstract

Research was performed to verify previously obtained friction coefficients for compressible, laminar and turbulent flow in a simulated heat pipe for intermediate mass injection and suction rates. The research was divided into two main parts: an experimental study and a numerical study.

In the experimental study, a simulated heat pipe consisting of a long porous tube with air injected into one end to simulate the evaporator and extracted from the other end to simulate the condenser was investigated. Axial static pressure variations for various air supply mass flow rates were measured. It was found that the friction in the pipe decreased the amount of pressure recovery at the end of the pipe and that this decrease became even greater with increased supply mass flow rate.

The pressure distributions obtained in the experimental study were used as input for a numerical simulation in the numerical portion of this research. A steady, one-dimensional computer code was developed to simulate the porous pipe system used in the experimental study in order to calculate Mach numbers, axial Reynolds numbers, and friction coefficients along the pipe. Newton's second law, continuity, and Shapiro's method of influence coefficients were used in the computer simulation to calculate the flow properties. The results

obtained for the friction coefficients in the porous pipe system studied did not correlate with the values predicted by Bowman's expressions. They did, however, exhibit the general trend expected for the friction coefficient - axial Reynolds number product with Mach number.

COMPRESSIBLE FRICTION COEFFICIENTS IN A SIMULATED HEAT PIPE

I. Introduction

The purpose of this introductory chapter is to acquaint the reader with the history and operation of the heat pipe and the goals of this research. The chapter is divided into three sections. The first section provides a brief discussion of the development and operation of the heat pipe, while in the second section the pertinent literature is reviewed. In the last section, the objectives of this study are outlined.

Development and Operation of the Heat Pipe

The concept of the heat pipe was first conceived by R.S. Gaugler in 1942 (4:1). The first serious development work took place many years later by G.M. Grover and his associates at the Los Alamos Scientific Research Laboratory in 1964 (4:1). Grover showed that the heat pipe is an effective high-performance heat transmitter, developed some applications for it, and gave it its present name. Following Grover's work, interest in the heat pipe quickly grew for both terrestrial and space applications, resulting in numerous papers and several books being written on the subject. Today heat pipes have numerous applications. Some of these applications include cooling nuclear reactors, infrared sensors, laser systems, generators,

electronic and electrical equipment, and turbine blades. Heat pipes have also been used for cyrogenic eye surgery, in spacecraft for temperature control of spacesuits and vehicles, and for heat collection from solar energy, geothermal energy, and exhaust gases.

The operation of the heat pipe is similar to that of the thermal syphon, shown in Figure 1.1. The thermal syphon consists of a sealed tube, from which the air has been evacuated, with a small quantity of liquid placed inside. When the end of the tube is heated, it causes the water to vaporize and move to the cooler end of the tube where it condenses on the walls. The condensate then returns to the other end of the tube by means of gravity. The thermal syphon is limited in its orientation since the evaporator region must be at the lowest end. The heat pipe, however, consists of a closed tube with a porous capillary wick fixed to the inside surface, in its conventional form (Figure 1.2). The wick contains the liquid phase of the working fluid while the remaining volume of the tube, known as the vapor region, contains the vapor phase of the working fluid. When heat is applied to evaporator end, the fluid in that section of the pipe is vaporized. This creates a pressure difference down the pipe and causes the vapor to flow from the evaporator end to the condenser end where the vapor condenses and releases its latent heat of vaporization to a heat sink. The evaporation process depletes the liquid in the evaporator section and causes the liquid-vapor interface to move into the wick

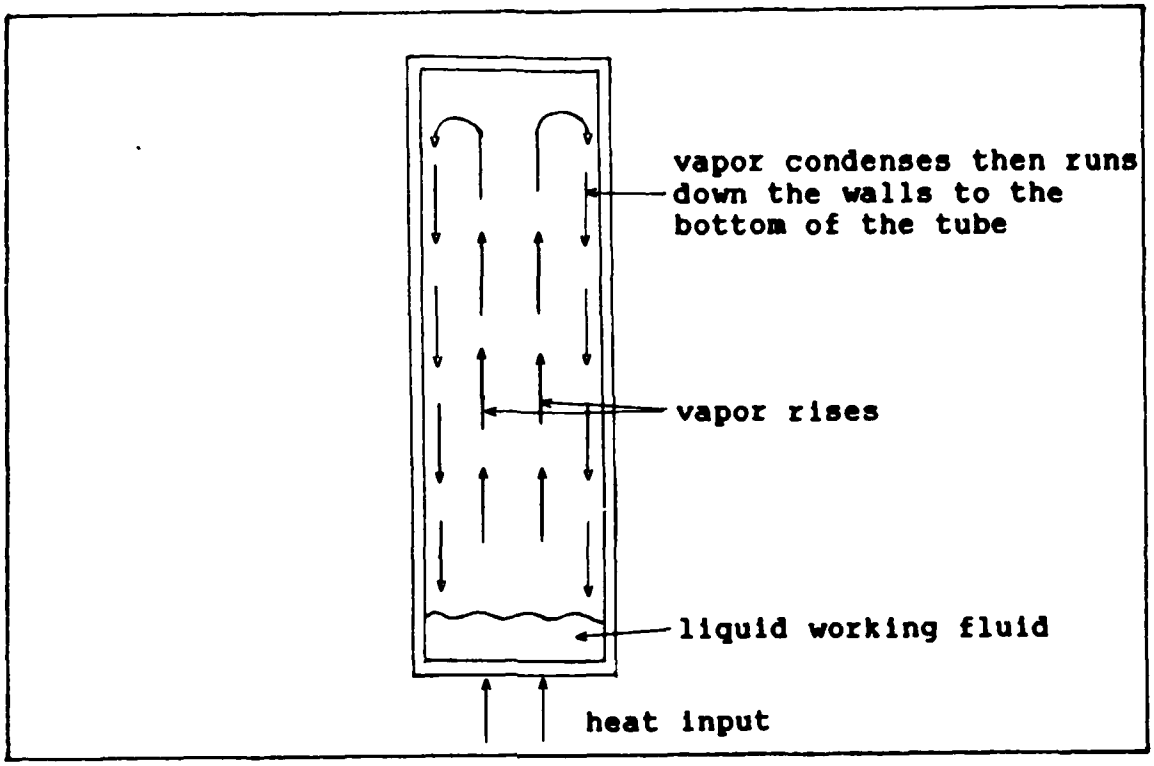

Figure 1.1 Diagram of the Thermal Syphon

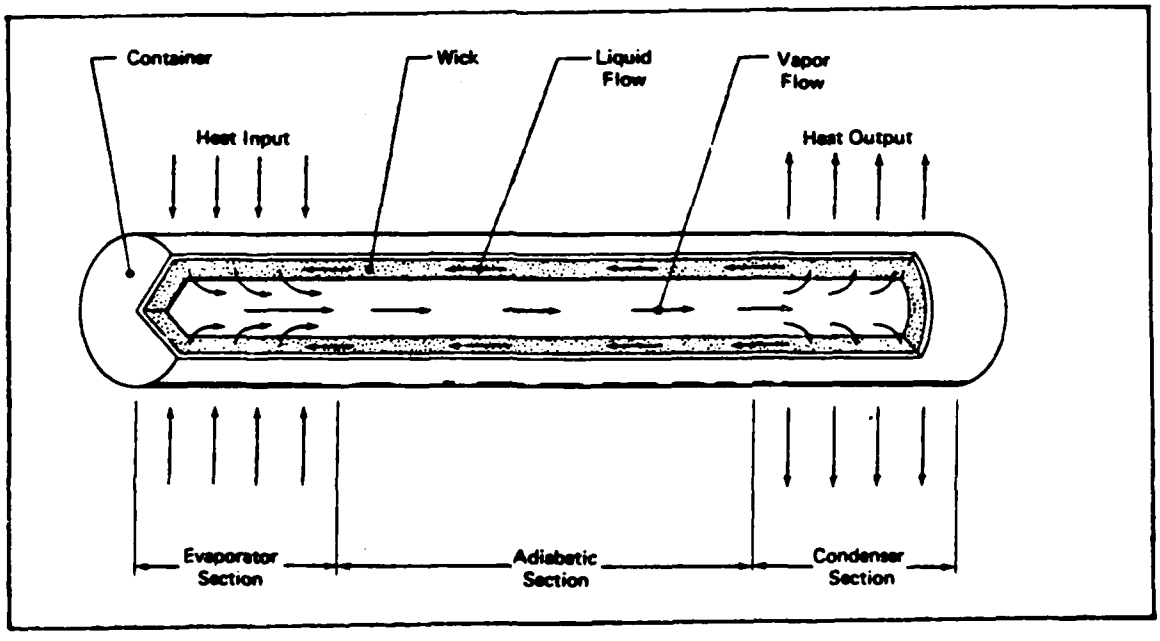

Figure 1.2 Components and Operation of a Conventional Heat Pipe (3:2)

surface, see Figure 1.3. A capillary pressure then develops which pumps the condensate back to the evaporator section. The quantity of heat capable of being transported as latent heat of vaporization is normally several orders of magnitude greater than the quantity that can be transported as sensible heat in a conventional convective system (3:1,2). This efficiency allows the heat pipe to transport large amounts of heat with a small size and a very small temperature difference between the two ends.

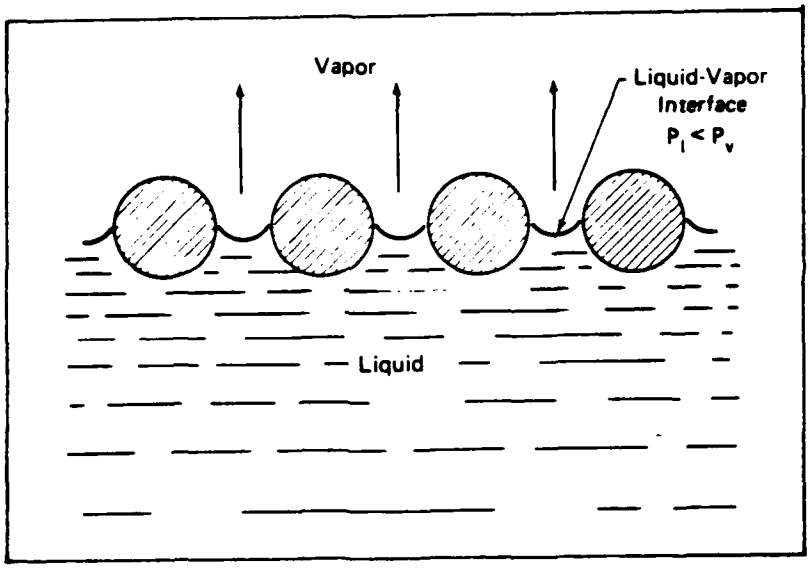

Figure 1.3 Development of Capillary Pressure at the Liquid-Vapor Interface (3:2)

Background Literature

As was stated in the previous section, numerous papers have been written on heat pipe theory and operation. This study is concerned primarily with the effect of mass injection and extraction on the friction coefficient at the tube wall.

Several articles have been written on this subject, but only a few of these will be discussed in this section.

Kinney (5) studied the effect of wall mass transfer on the frictional and heat transfer characteristics of fully developed laminar flow in circular porous tubes. His results are based on the assumptions of a constant-property fluid and uniform wall mass transfer and are presented for radial Reynolds numbers (Reynolds numbers based on the velocity of the flow through the tube wall and the tube diameter) ranging from -4.618 to 20. Using numerical solutions to the tube flow and energy equations, he found that the friction coefficient, f, was a function of both the radial and axial Reynolds numbers, Re_w and Re_x, respectively. For large values of Re_w, the values of the product f*Re asymptotically approached the value 19.739. He also found that the wall friction decreased with increased extraction radial Reynolds number and that for a given axial Reynolds number fluid injection caused an increase in the wall friction.

Yuan and Finkelstein (11) studied the effects of uniform wall injection and extraction on two-dimensional laminar incompressible flow in a tube with porous walls. They used a perturbation method to solve the Navier-Stokes equations in cylindrical coordinates, and they observed that fluid injection at the wall accelerated the main stream velocity and thus increased the velocity gradient at the wall. The wall frictional coefficient was therefore found to increase with injection and decrease with suction.

Kinney and Sparrow (6) used an analytical model to investigate the effects of surface suction on friction, heat transfer, and mass transfer for turbulent flow inside a tube. They found that the shear force was greater when suction was present than when it was absent and that high Reynolds number flows are more sensitive to suction than low Reynolds number flows. They also observed that in the presence of suction the momentum change of the flow tended to increase the pressure in the flow direction, while the wall shear stress tended to decrease the pressure.

For his doctoral dissertation at the Air Force Institute of Technology in 1986, Bowman numerically and experimentally investigated the effects of mass injection and extraction on the wall frictional coefficients (2). Bowman developed functional relationships for friction coefficients to be used in one-dimensional heat pipe vapor models to design heat pipes for compressible-flow situations with large mass injection and extraction rates. Bowman used a simulated heat pipe with air as the working fluid and found that the friction coefficient in general is a function of Re_w, Re_∞, Mach number and the ratio of pipe length to diameter. For laminar flow, he found the relationship to be

$$f^*Re_\infty = 16(1.2337 - 0.2337 \exp(0.0363Re_w)) \times \exp(6Ma^2/5) \quad (1.1)$$

and for turbulent flow

$$f = f^*[\ 1 + 55\ Re^{0.1}(v/u)^{0.9}(2L_c/D)^{0.1}\exp(6Ma^2/5)] \quad (1.2)$$

where

$$f^* = 0.046/Re^{1/5} \quad (1.3)$$

where v is the radial velocity, u is the average axial velocity, D is the pipe inside diameter, and L_c is the length of the condenser.

Objective and Scope

The main objective of this research is to verify Bowman's friction coefficient expressions for intermediate radial Reynolds number compressible flow. To accomplish this, a simulated heat pipe and a numerical simulation were used. The axial pressure variation was experimentally measured along the simulated heat pipe. This pressure distribution was used as input to a numerical model designed to model one-dimensional compressible and incompressible flow in a tube with mass injection and extraction. The numerical model utilized the pressure distribution to solve for the friction coefficient distribution along the pipe. For axial flow Mach numbers less than 0.01, Newton's second law and incompressible flow equations were used to solve for the flow properties; while for Mach numbers greater than 0.01, compressible flow, the continuity equation and Shapiro's method of influence coefficients (9) were employed. The numerical results were then compared to the values predicted by Bowman's expressions.

II. Experimental Model

The purpose of the experimental portion of this study was to obtain data on the pressure distribution for flow inside a simulated heat pipe at intermediate radial Reynolds numbers. This was accomplished by means of a simulated heat pipe modeled after the one used by Bowman (2) in his research. The sample pressure distributions were then used as input to a numerical model, to be discussed in Chapter III, in order to calculate the friction coefficient distribution. This chapter discusses how the heat pipe vapor flow was simulated and the experimental configuration used to model the flow.

Heat Pipe Simulation

A simulated heat pipe was used because of its advantages over an actual heat pipe in experimental studies. The design consisted of two porous pipes of equal length placed end to end with air injected through the walls of one pipe to model the evaporator and extracted through the walls of the other pipe to model the condenser. Wageman and Guevara (10) and Quale and Levy (8) showed that this system simulates the vapor dynamics in a heat pipe quite well. One advantage of the simulated heat pipe is that it is much simpler to build and test. Heat pipes typically operate at low pressures with very small axial pressure gradients, making it difficult to measure pressures. The porous pipe system eliminates this problem since it operates at higher pressures with larger pressure gradients,

yet still accurately simulates flow in an actual heat pipe. In addition, this system does not require complicated heating and cooling equipment nor does it require a liquid return mechanism (similar to a wick in a heat pipe).

Experimental Apparatus

As was mentioned earlier, the experimental set up used in this investigation was modeled after that used by Bowman. Much of the same equipment he used was used for this experiment as well; for this reason, only a brief discription of the set up will be given. The reader is referred to Bowman's dissertation for additional details.

In order to obtain intermediate radial Reynolds numbers a longer porous pipe with a smaller diameter than that used by Bowman was required. A polyethylene porous pipe produced by Porex Technologies with a nominal pore size of 35 microns, a 5/8 inch inside diameter and 3/4 inch outside diameter was the smallest diameter pipe found. Since this pipe was only slightly smaller in diameter than Bowman's, the length of the test section was increased to approximately seven feet. The pipe selected was only available in four foot lengths; therefore, two four foot pipes were chosen. One three inch section was cut from both ends of each pipe for calibration tests leaving two 3-1/2 foot pipes. One pipe was used to model the evaporator and was enclosed in a manifold designed and built to supply the air for injection. The injected air was passed through a filter just prior to entering the test configura-

tion. The other pipe, used to model the condenser, was left open to the atmosphere. A diagram of the set up is shown in Figure 2.1. The two pipes were placed end to end so that the air injected into the first porous pipe would flow into the second pipe where it would be extracted through the walls of the pipe into the atmosphere.

In the original test configuration, twelve pressure taps were installed, six evenly spaced in each pipe. When pressure measurements were made, it was found that the pressure varied along the tube more than expected in the condenser section; so 15 additional pressure taps were added to that section. The final configuration is shown in Figure 2.1. Twenty-seven pressure taps were used in the porous pipes, six in the evaporator section spaced six inches apart and twenty-one in the condenser section spaced every two inches. In addition, five other pressure taps were used in the system. Two were used to measure the pressure around the orifice plate, one above the plate and one below the plate. One tap was used to measure the pressure at the upstream end of the air supply manifold and two taps were used to measure the pressure at the downstream end of the manifold. Stainless steel 0.060 inch outside diameter tubes were used as pressure taps. The tubes were inserted and cemented into 0.058 inch diameter holes in the porous pipe to produce a tight fit. The stainless steel tubes were installed such that their ends were flush with the inside wall of the porous pipe.

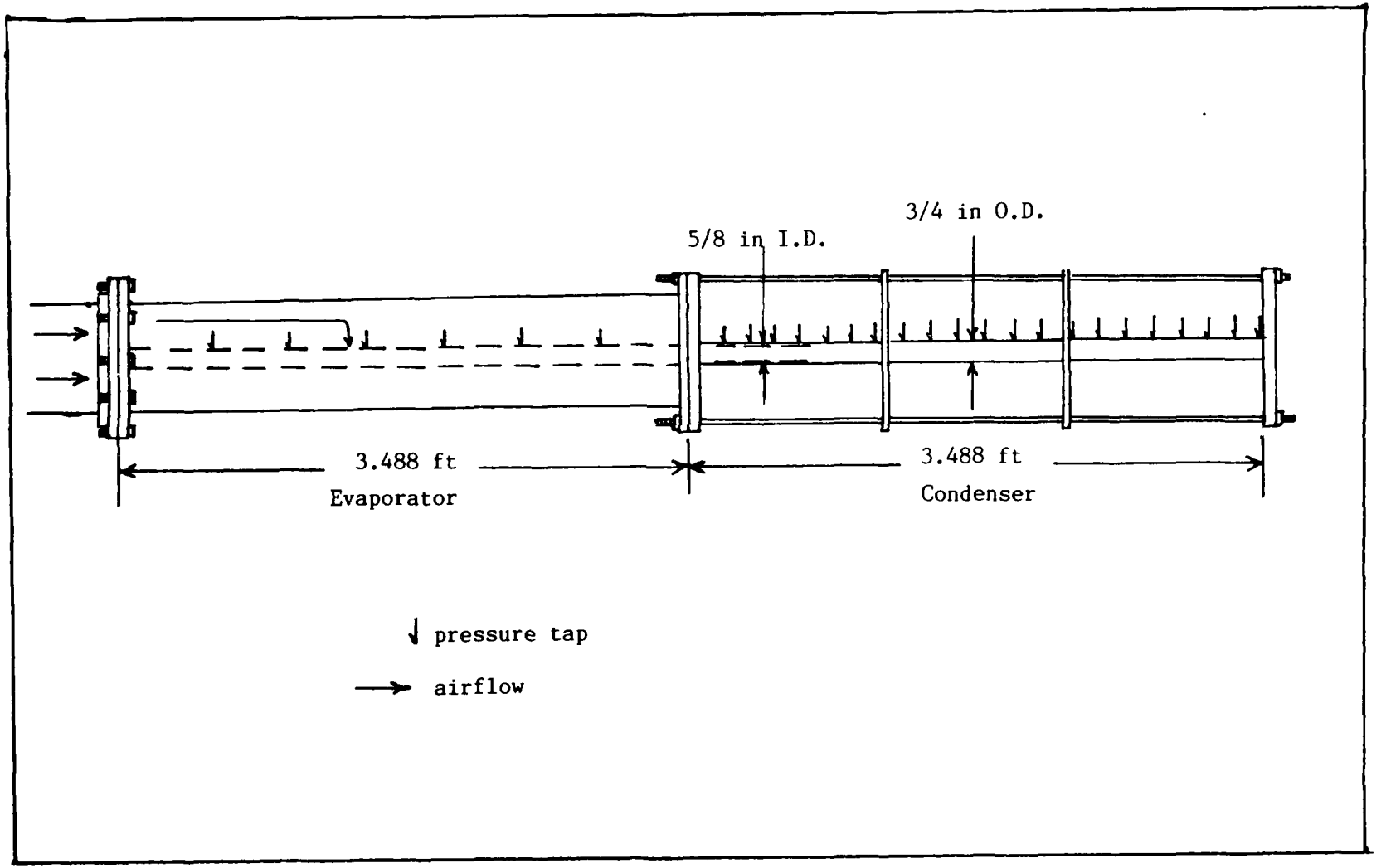

Figure 2.1 Experimental Test Configuration

Pipe Calibration

The calibration of the porous pipe was made using a relationship developed by M. Muskat (7:66). Muskat found that the mass flux through a porous medium is related to the pressure difference across the porous medium by the following expression:

$$(\Delta p^2) = A(\rho v)^2 + B(\rho v) \qquad (2.1)$$

Each of the four porous pipe samples taken from the pipe used in the test configuration were installed into the test manifold designed by Bowman (Figure 2.2). For each sample, Δp^2 and ρv were measured at various mass flow rates. The

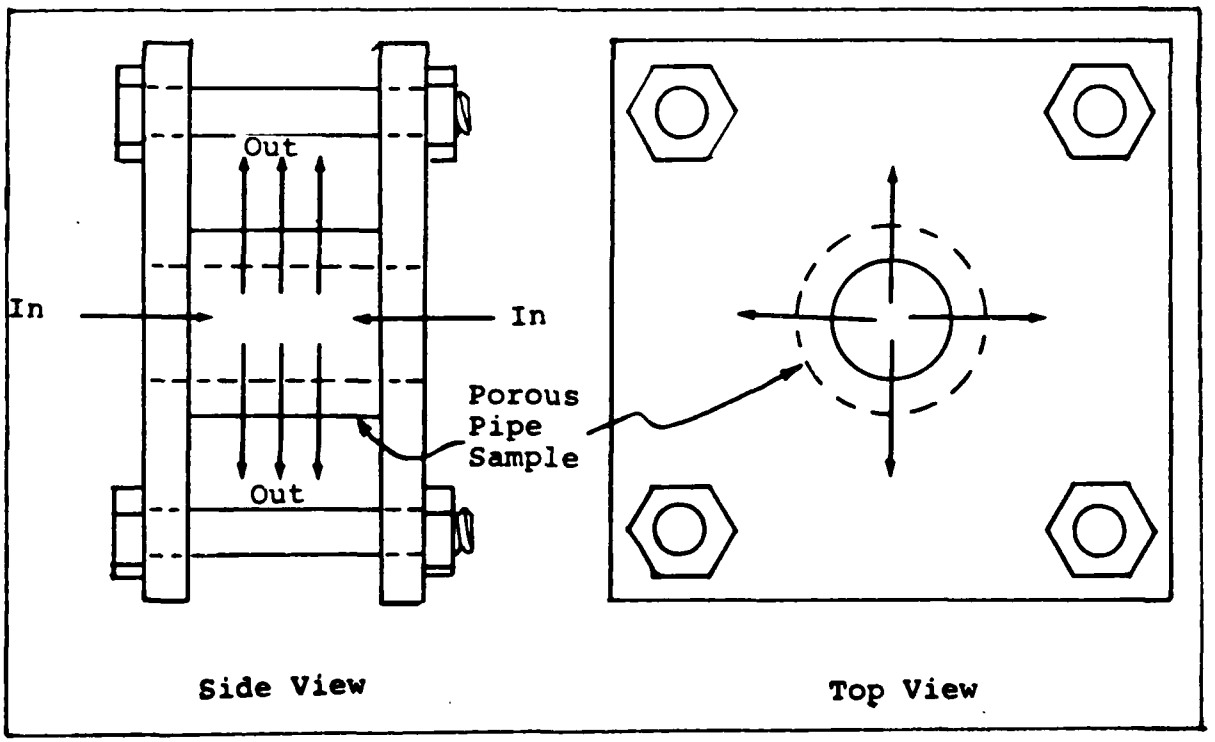

Figure 2.2 Porous Pipe Calibration Manifold (Bowman 2:29)

curve was expected to be very close to linear at very low mass flow rates, with the contribution of the $A(\rho v)^2$ term being quite small compared to the $B(\rho v)$ term. This linear behavior was observed in that region, however the curve was offset from the origin by the amount $\Delta p^2 = 126{,}921.84$ lbf^2/ft^4. These results are shown in Figure 2.3. This offset in the curve was probably due to the tendency of the pressure transducer in the Scanivalve to read the pressures higher than what they actually were. The atmospheric pressure readings made by the Scanivalve were consistently higher than those taken from the barometer in the laboratory. To correct for this effect, the offset value was subtracted from each ΔP^2 reading. The values for the constants A and B in Equation (2.1) were calculated using a least squares technique to curve fit the corrected calibration data and were found to be 4.679×10^6 ft^2/sec^2 and 4.2843×10^7 lbf/ft-sec, respectively. The final calibration results are shown in Figures 2.4 and 2.5. Figure 2.5 is an enlargement of the region of the graph in Figure 2.4 for the low mass flow rates. Equation (2.1) was needed for the numerical model to determine the mass flux for a given pressure differential across the pipe walls.

Data Measurement and Acquisition

A Zenith Z-100 computer was used for the data acquisition. Pressure measurements were made using a T-type Scanivalve, from Scanivalve Corporation, with a model PDCR42 differential pressure transducer having a pressure range of -100 to 100

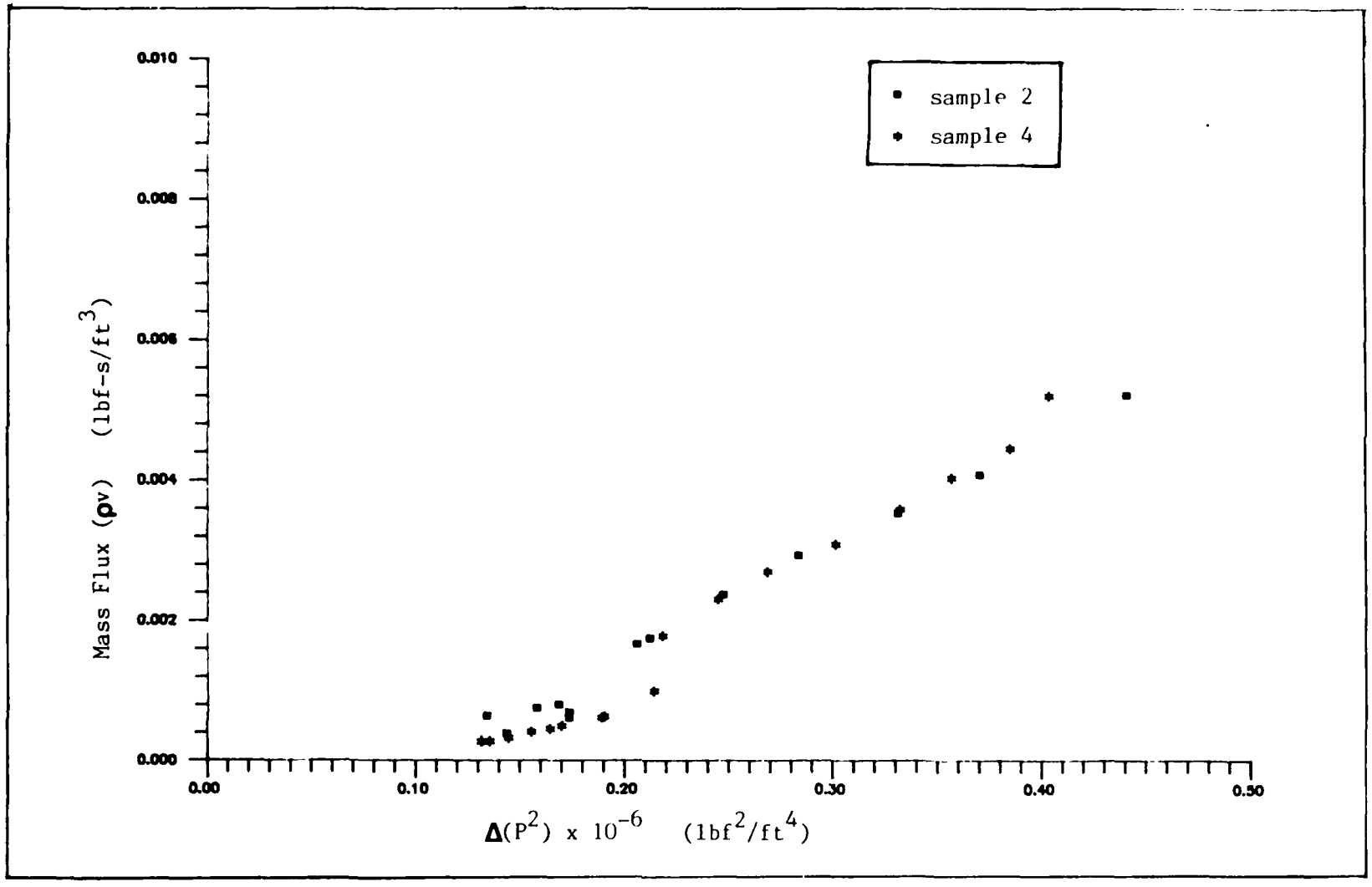

Figure 2.3 Porous Pipe Calibration Data Showing Offset From Origin

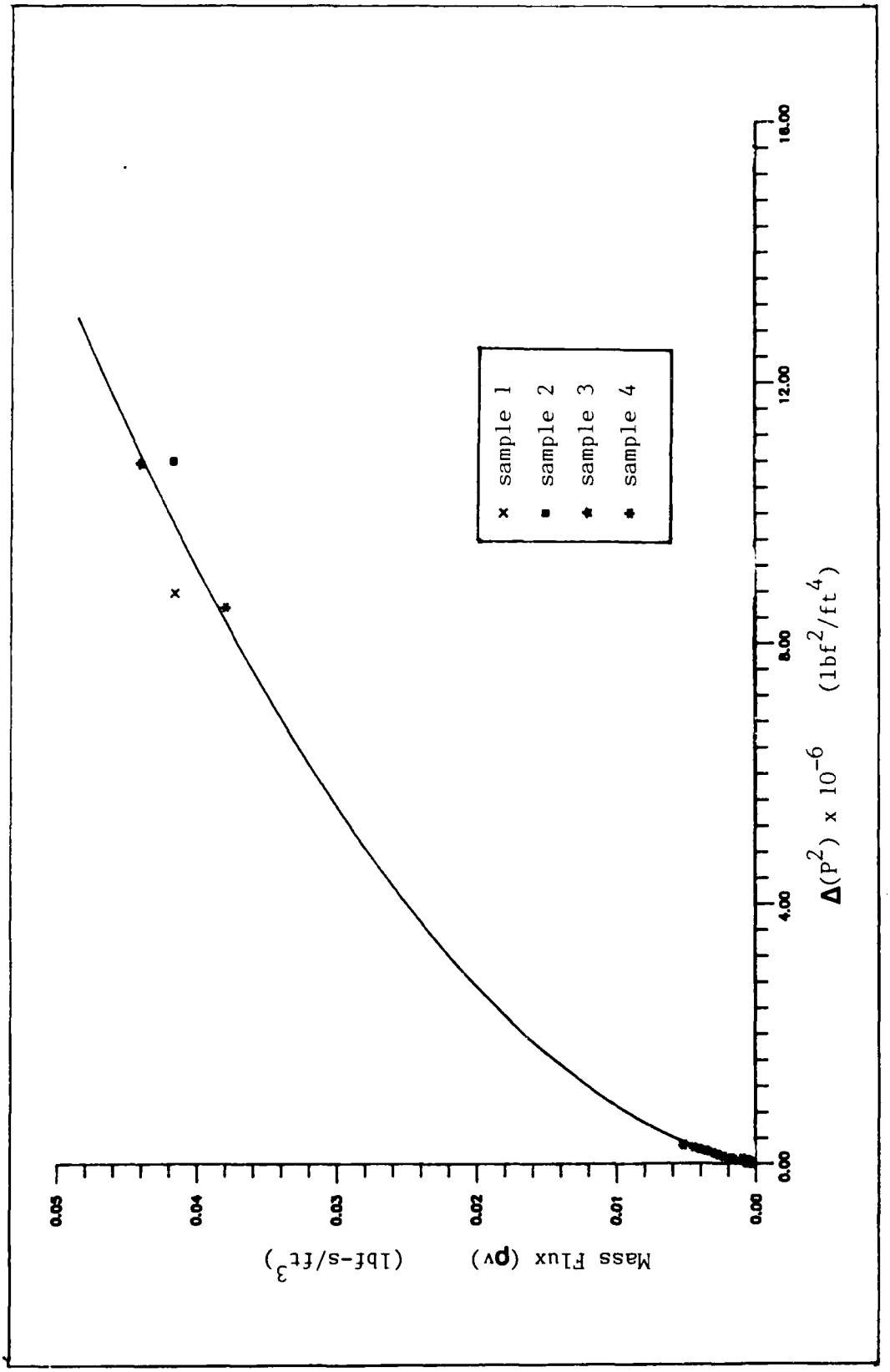

Figure 2.4 Porous Pipe Calibration Results

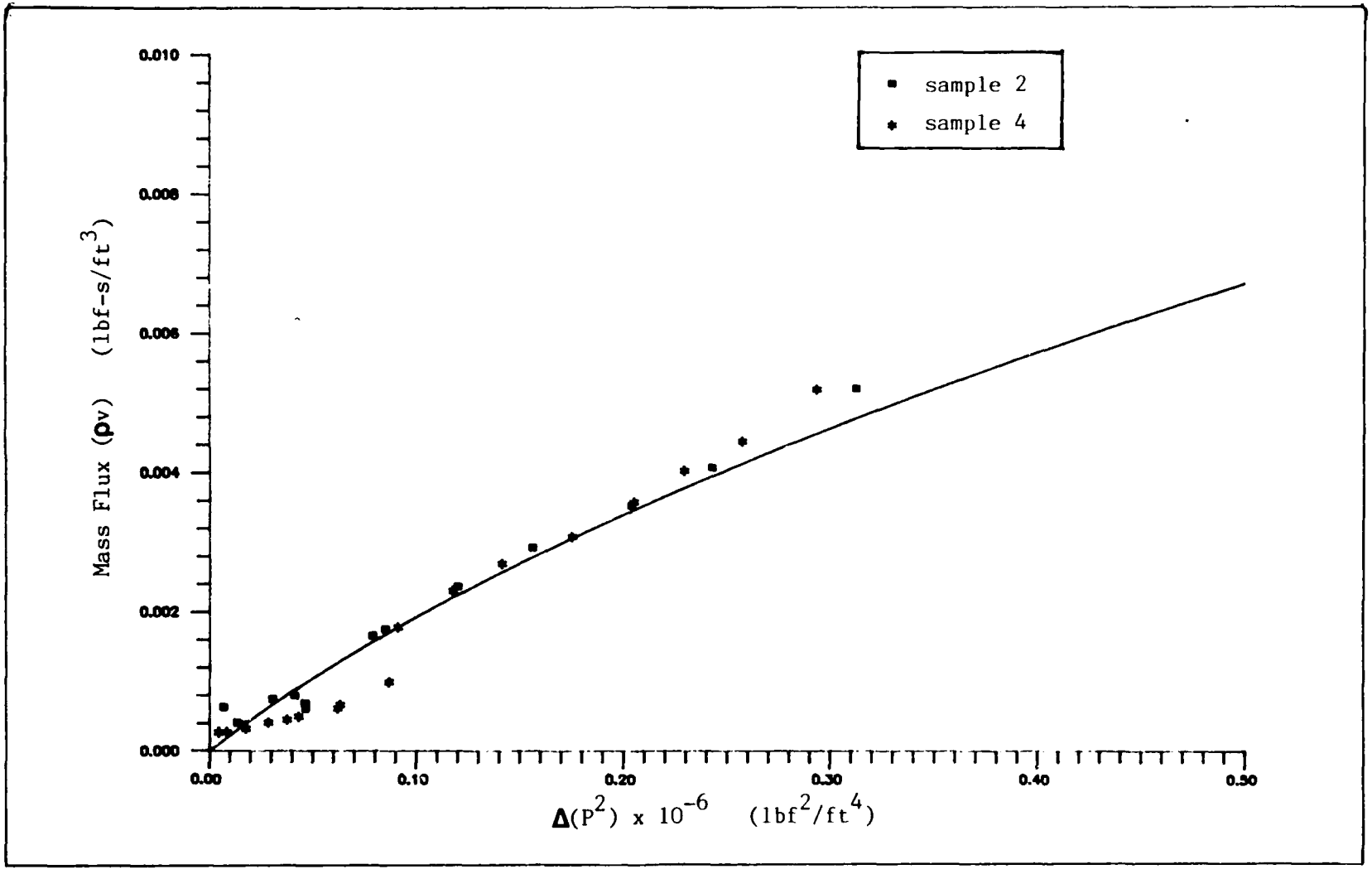

Figure 2.5 Enlargement of $\Delta(P^2)$ Range 0 - 500,000 lbf^2/ft^4 in Calibration Results

psig. A Dual Systems Control model AIM12 analog-to-digital card in the computer was used to digitize the pressure transducer input into the computer. The offset option on the card and amplification were set to read signals from -100 to +100 mV with a resolution of 0.048 mV. Fifty data samples were averaged for each point to reduce noise. For mass fluxes above 0.035 lbf-sec/ft^3, a square-edged orifice plate was used to measure the total mass flow rate entering the test configuration. The pressure differential across the orifice plate was measured using both the Scanivalve and a water manometer. The mass flow rate was calculated using the following expression (1):

$$\dot{m} = 0.52502(CYd^2F_a)(\rho_1(p_1 - p_2)^{1/2}/(1 - \beta_a^4) \qquad (2.2)$$

where

$$C = K/E = K(1 - \beta_a^4)^{1/2} \qquad (2.3)$$

$$K = K_\infty(1 + A/Re_d) \qquad (2.4)$$

$$K_\infty = K_L[10^6 d/(10^6 d + 15A)] \qquad (2.5)$$

$$K_L = .5993 + .007/D + (.364 + .076/D^{1/2})\beta_a + .4(1.63 - 1/D)[(.07 + .5/D) - \beta_a]^{3/2} - (.009 + .034/D)(.5 - \beta_a)^{3/2} + (65/D^3 + 3)(\beta_a - .7)^{3/2} \qquad (2.6)$$

$$A = d(830 - 5000\beta + 9000\beta^2 - 4200\beta^3 + 530/D^{1/2}) \qquad (2.7)$$

$$Y = 1 - (.41 + .35\beta_a^4)(X/k) \qquad (2.8)$$

$$X = P/P_1 \qquad (2.9)$$

$$Re_d = 4\dot{m}/\pi\mu d \qquad (2.10)$$

Very low mass flow rates, such as those measured in the calibration tests, were measured using a flowmeter with a range of 0 to 0.44 cfm. The pressure was measured at a point just upstream of the flowmeter in order to calculate the density of the air. In addition, a valve was installed just downstream of the flowmeter to vary the upstream pressure in order to read higher mass flow rates with the meter. It was important to get accurate readings in the low mass flow rate region because there were several sections of the simulated heat pipe where the injection/suction rates were quite small. Equation (2.1) with the constants A and B calculated from data for mass fluxes only above 0.04 lbf-sec/ft^3 underpredicted the mass fluxes at low Δp^2.

Experimental Results

The pressure variation obtained along the pipe was a result of two effects: the friction encountered along the pipe walls and the rate of change in momentum along the pipe. The total effect of the friction force was manifested in the pressure drop between the two ends, or the lack of complete pressure recovery. The pressure drop due to friction was found to increase with increased mass flow rate. Figure 2.6 shows the pressure distribution for five different mass flow rates. Additional data for other mass flow rates can be found in Appendix A. As mass was added in the evaporator region, $0 < X/L < 0.5$, the fluid accelerated with increasing X/L with a corresponding drop in pressure. The mass removal

in the condenser section caused the flow to decelerate and the pressure to rise.

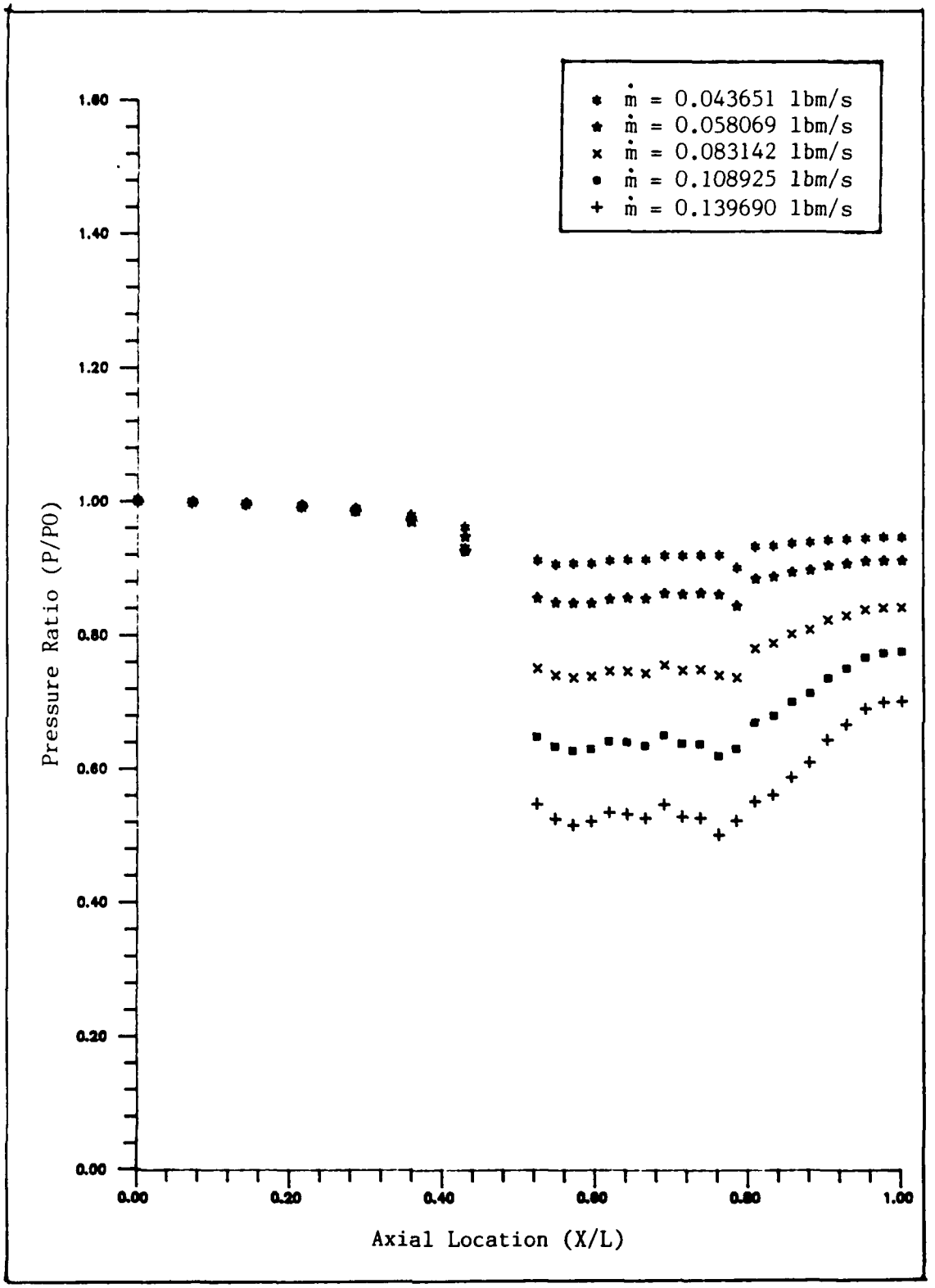

Figure 2.6 Axial Pressure Distributions

III. Numerical Model

This chapter describes the numerical model used to simulate the flow generated by the experimental model. The governing equations used to solve for the flow properties will be discussed first, followed by a discription of the solution technique used. Finally, the results obtained will be presented.

Governing Equations

All of the flowfields generated with the experimental configuration contained sizable regions of very low Mach number (Ma < 0.1). Therefore, two models were used in the numerical simulation: an incompressible model for Mach numbers less than 0.01, and a compressible model for Mach numbers greater than 0.01. One-dimensional, steady, adiabatic flow was assumed for both models.

Incompressible Model. The incompressible model consisted primarily of Newton's second law and incompressible flow relations. To approximate the shear stress at the pipe wall, Newton's second law was applied to an element of fluid in the pipe (Figure 3.1).

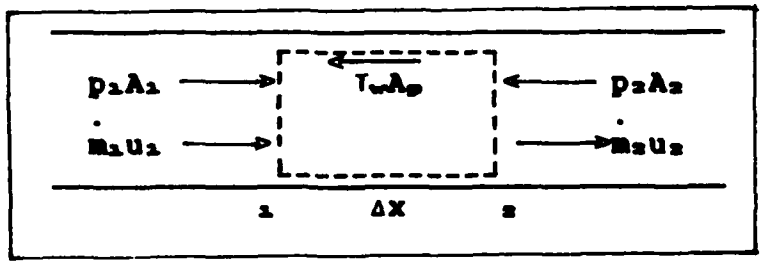

Figure 3.1 Element of Fluid for Equation of Motion

Applying Newton's second law for steady flow to the fluid element gives

$$\dot{m}_2 u_2/g_c - \dot{m}_1 u_1/g_c = (p_1 A_1 - p_2 A_2) - \tau_w A_p \qquad (3.1)$$

where A_p is the wall surface area for the increment Δx. Equation (3.2) can be solved for τ_w giving

$$\tau_w = [\, \dot{m}_1 u_1/g_c - \dot{m}_2 u_2/g_c + (p_1 - p_2)A_c \,]/A_p \qquad (3.2)$$

where A_c is the cross-sectional area equal to A_1 and A_2. The expression for the friction coefficient is given by

$$f = 2\, \tau_w\, g_c/\, \rho \bar{u}^2 \qquad (3.3)$$

where

$$\bar{u} = (u_1 + u_2)/2 \qquad (3.4)$$

Substituting the expression for τ_w given by Equation (3.2) in Equation (3.3) gives an expression for the friction coefficient in terms of quantities which can be calculated from the input pressure distribution

$$f = 2[\, \Delta M + (p_1 - p_2)A_c \,]g_c/\, \rho \bar{u}^2 A_p \qquad (3.5)$$

where

$$\Delta M = \dot{m}_1 u_1/g_c - \dot{m}_2 u_2/g_c \qquad (3.6)$$

The axial velocities along the pipe were calculated from a mass balance on an element of fluid in the pipe (Figure 3.2).

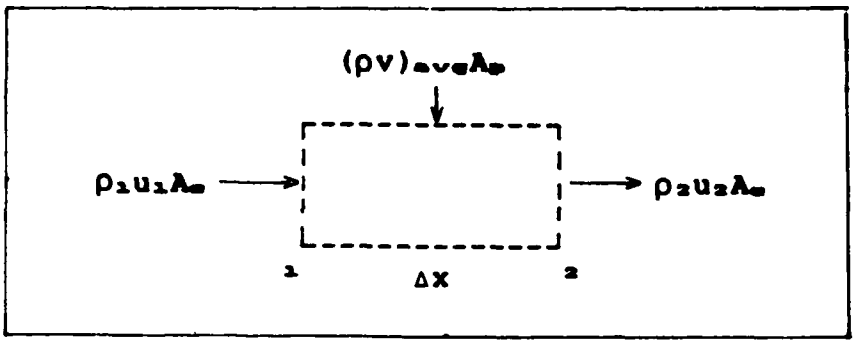

Figure 3.2 Element of Fluid Used For Mass Balance

Performing the mass balance on the fluid element in Figure 3.2

$$\rho_2 u_2 A_m = \rho_1 u_1 A_m - (\rho v)_{avg} A_p \qquad (3.7)$$

where $(\rho v)_{avg}$ is the average mass flux through the pipe walls over the increment Δx found by applying Equation (2.1) at stations 1 and 2 (shown in Figure 3.2) and taking the average of the two. The negative sign on the quantity $(\rho v)_{avg}$ is a result of the sign convention on the mass flux. For injection, (ρv) is considered negative and considered positive for suction. Equation 3.7 can be solved for u_2 giving

$$u_2 = \rho_1 u_1 / \rho_2 - (\rho v)_{avg} A_p / \rho_2 A_m \qquad (3.8)$$

The velocity u_1 is taken from the previous step and its initial value is zero.

The pressure at each step was found by interpolating from the input pressure distribution using a second degree interpolation formula. Figure 3.3 illustrates this interpolation procedure.

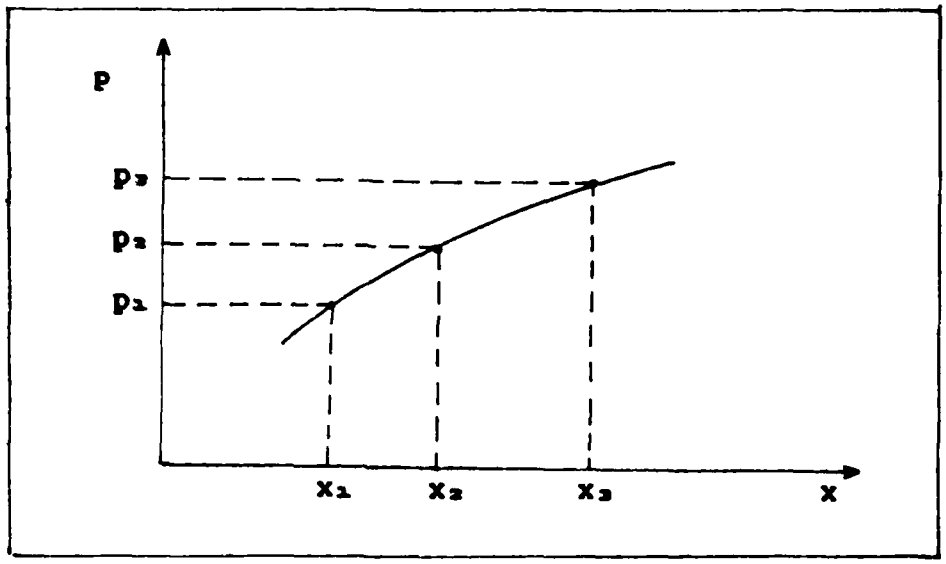

Figure 3.3 Pressure Interpolation

Refering to Figure 3.3 for $x_1 < x < x_3$, p(x) is given by

$$p(x) = p_1K_1 + p_2K_2 + p_3K_3 \qquad (3.9)$$

where

$$K_1 = [(x - x_2)(x - x_3)]/[(x_1 - x_2)(x_1 - x_3)]$$
$$K_2 = [(x - x_1)(x - x_3)]/[(x_2 - x_1)(x_2 - x_3)] \qquad (3.10)$$
$$K_3 = [(x - x_1)(x - x_2)]/[(x_3 - x_1)(x_3 - x_2)]$$

The temperature (T), viscosity (μ), axial Reynolds number (Re_m), and radial Reynolds number (Re_w) were calculated from the following expressions:

$$T = T_o/[\ 1 + (k - 1)Ma^2/2\ ] \qquad (3.11)$$

$$\mu = 2.27E\text{-}08\ (T)^{3/2}/(T + 198.6) \qquad (3.12)$$

$$Re_m = 4\ \dot{m}_{avg}\ /(\pi\ D\ \mu\ g_o) \qquad (3.13)$$

$$Re_w = (\rho v)_{avg}\ D\ /(\ \mu\ g_o) \qquad (3.14)$$

where T in Equation (3.11) is in degrees Fahrenheit, and $\dot{m}_{avg}$

is the average of m_1 and m_2. Equations (3.5), (3.8) - (3.14), and (2.1) thus comprise the equations for the incompressible model.

Compressible Model. The compressible model consisted of Equations (3.9) - (3.14) along with the differential form of the continuity equation and Shapiro's method of influence coefficients for Mach number variation with friction and wall mass transfer to solve for the velocity and friction coefficient, respectively. The differential form of the continuity equation in terms of pressure, temperature and Mach number is given by

$$\frac{\dot{dm}}{\dot{m}} = \frac{d\rho}{\rho} + \frac{dMa}{Ma} + \frac{1}{2}\frac{dT}{T} \qquad (3.15)$$

Using the equation of state for an ideal gas, $\rho = p/RT$, and Equation (3.11) in equation 3.15 gives the differential form of the continuity equation in terms of pressure and Mach number.

$$\frac{\dot{dm}}{\dot{m}} = \frac{dp}{p} + \frac{1}{2}\left[\frac{1 + (k-1)Ma^2}{1 + (k-1)Ma^2/2}\right]\frac{d(Ma)^2}{Ma^2} \qquad (3.16)$$

Equation (3.16) can then be integrated to solve for Ma_2 , which is given by the following expression

$$Ma_2^2 = \{-1 + [1 + 2(k-1)C]\}/(k-1) \qquad (3.17)$$

where

$$C = Ma_1^2\,[1 + (k-1)Ma_1^2/2\,](\dot{m}_2/\dot{m}_1)^2/(p_2/p_1)^2 \qquad (3.18)$$

The equation for Mach number variation with friction and wall mass transfer utilizing Shapiro's method of influence coefficients is given by

$$d(Ma^2)/Ma^2 = F_s 4f\, dx/D + F_w\, \dot{dm}/\dot{m} \qquad (3.19)$$

where F_s and F_w are the influence coefficients defined by

$$F_s = Ma^2[1 + (k - 1)Ma^2/2]/(1 - Ma^2) \qquad (3.20)$$

$$F_w = 2(1 + kMa^2)[1 + (k - 1)Ma^2/2]/(1 - Ma^2) \qquad (3.21)$$

where x is the axial coordinate. Equation (3.19) can be rearranged into the following form

$$\frac{(1 - Ma^2)\, dMa^2}{kMa^2[1 + (k - 1)Ma^2/2]} = \frac{4fdx}{D} + \frac{2(1 + kMa^2)}{kMa^2}\frac{\dot{dm}}{\dot{m}} \qquad (3.22)$$

Equation (3.22) is in a form which can be integrated to yield an expression for the friction coefficient. After performing the integration and rearranging, the following expression results

$$f = D[\ \ln(Ma_1^2/Ma_2^2) - C_m \ln(p_2/p_1)]/(2\Delta x) \qquad (3.23)$$

where

$$C_m = (1 + k\overline{Ma^2})/(k\overline{Ma^2}) \qquad (3.24)$$

$$\overline{Ma^2} = (Ma_1^2 + Ma_2^2)/2 \qquad (3.25)$$

and where Ma_2^2 is found from Equation (3.17) and Ma_1^2 is taken from the previous step. Equations (3.9) - (3.15), (3.17), (3.23) and (2.1) form the set of equations used in the compressible model.

Solution Method

A marching technique was used to solve for flow properties along the simulated heat pipe. The pressure information obtained from the experimental work was first read in to the program; then the various constants for the pipe geometry and the air properties and the variables at the upstream end of the pipe were set. The set of equations for the incompressible model were then solved to find the Mach number, axial Reynolds number, and friction coefficient for each Δx increment along the pipe until a Mach number of 0.01 was reached. After that, the compressible model equations were used to determine the properties. Sample calculations for the first iteration made by the program are given in Appendix B and a copy of the code used is included as Appendix C.

To verify the accuracy of the numerical simulation, three checks were made in the program. The first check was a comparison of the mass flow rate entering the condenser with the mass flow rate entering the air supply manifold for the evaporator to see if the two were equal. The second check was a force balance over the entire pipe. When considering the pipe as a whole, the only forces acting on the fluid are the pressures at the two ends and the total wall shear force (see Figure 3.4).

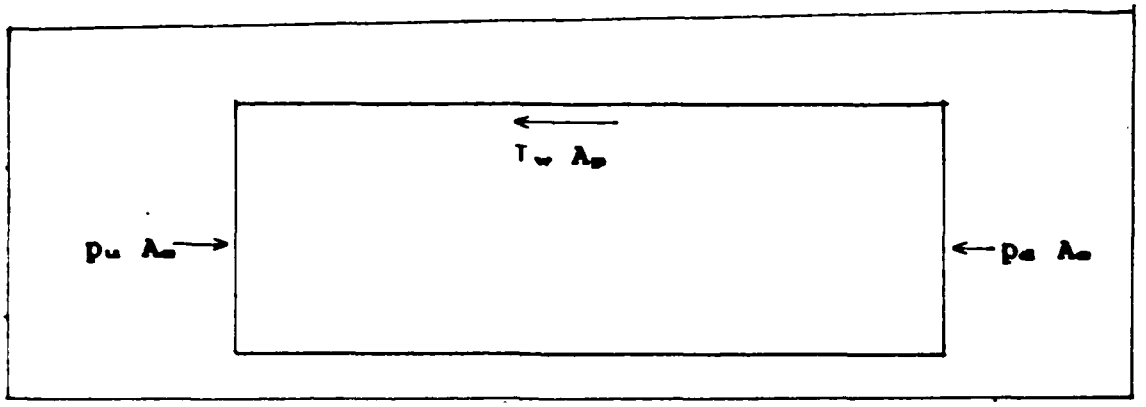

Figure 3.4 Force Balance on Entire Heat Pipe

A summation of these forces gives

$$\Sigma F = (p_u - p_d)A_c - \tau_w A_p \qquad (3.26)$$

where A_p is the surface area of an increment Δx of pipe. Ideally, this summation should be zero, since the drop in pressure between the two ends of the pipe is a result of the wall shear stress. The last check made was a mass balance over the entire pipe to see if the total mass injected into the pipe equaled the total mass removed from the pipe.

Numerical Results

All of the numerical simulations made using the code in Appendix C modeled the porous pipe system used in the experimental study for various supply mass flow rates. The results are plotted as the friction coefficient - axial Reynolds number product (f^*Re) versus Mach number for the evaporator in Figure 3.5 and for the condenser in Figure 3.6.

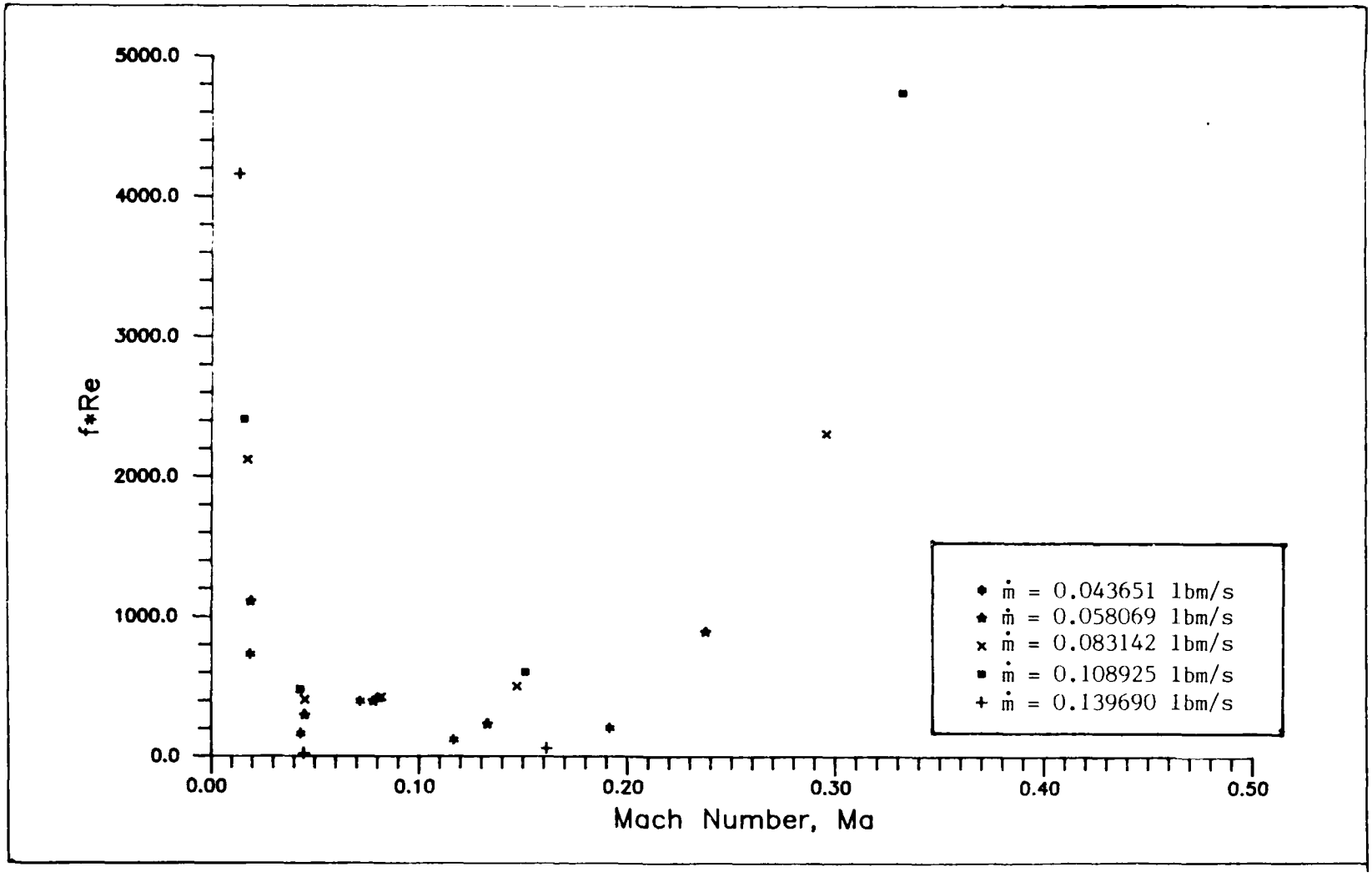

Figure 3.5 Effect of Compressibility in Evaporator

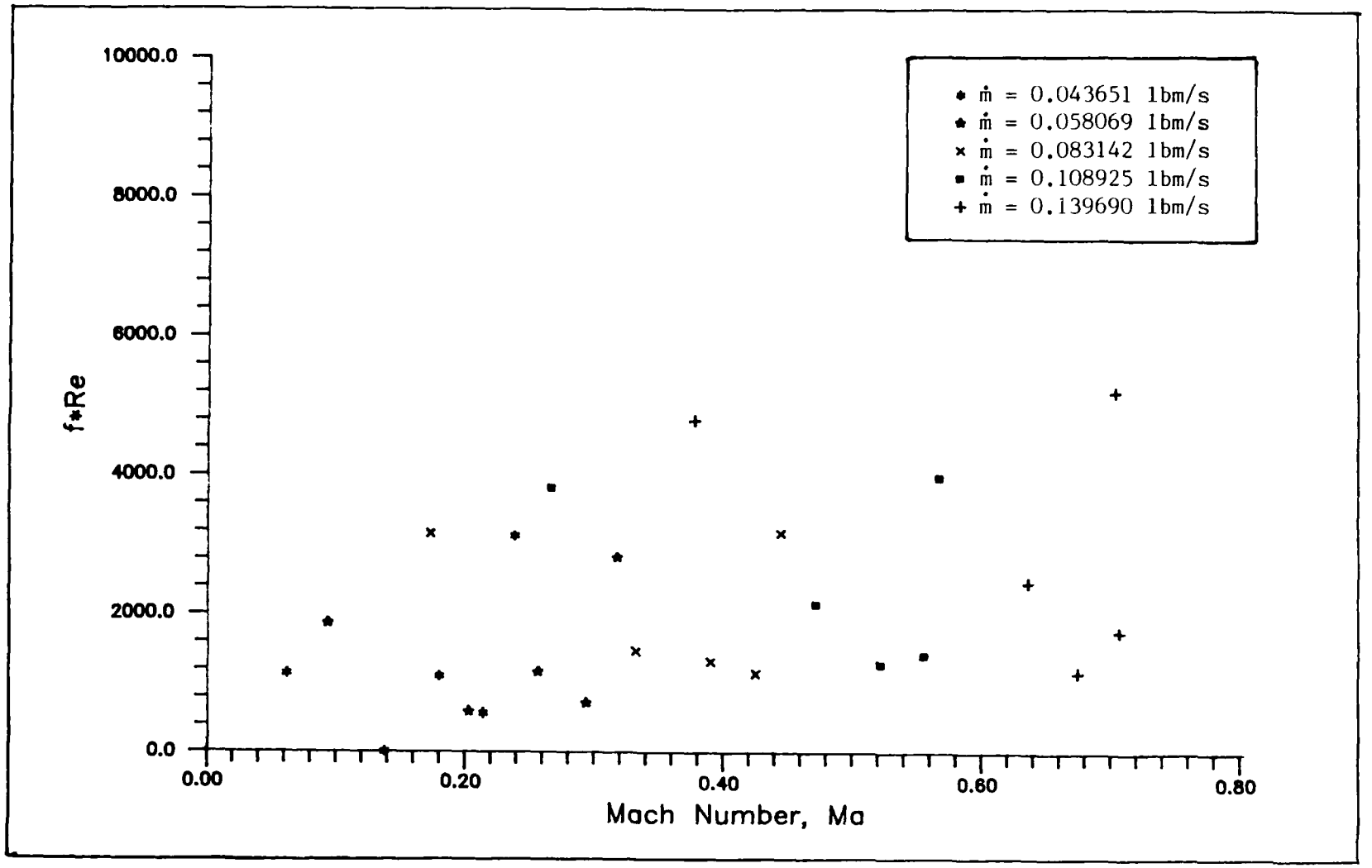

Figure 3.6 Effect of Compressibility in Condenser

IV. Discussion of Results

This chapter discusses the results obtained in both the experimental and numerical portions of this research. The reader is referred to Figure 2.6 for the discussion of the experimental results and to Figures 3.5 and 3.6 for the discussion of the numerical results.

Experimental Results Discussion

An important part of the experimental study was the calibration of the porous pipe. It was particularly important to obtain accurate data for the very low mass flux range, 0.0 - 0.005 lbf-sec/ft^3, since the simulated heat pipe operated with several regions of very low mass flux. The four pipe samples taken from the porous pipe used in the test configuration were originally calibrated using the orifice plate-water manometer system (described in Chapter II) to measure the mass flow rate entering the test sample. This system only allowed measurements of mass flow above approximately 0.03 lbf-sec/ft^3, since the ratio of the orifice plate bore to the air supply pipe diameter was 0.327 and values of the discharge coefficient are not available for ratios below 0.3. Curve-fitting the data from these first calibration tests produced values for the constants A and B in Equation (2.1) which under-predicted the mass flux for small values of Δp^2. Further calibration tests were then made on two of the four samples, one sample from the pipe used in the evaporator section and one

from the pipe used in the condenser section, using a flowmeter with a range of 0 - 0.44 cfm. Only two of the samples were calibrated because the other two were too dirty and clogged from the first set of calibration tests to yield accurate results. The data obtained from the second set of calibration tests exhibited the linear behavior expected in the low mass flux region, but the curve showed an offset from the origin, where it should have passed through. This offset probably resulted from a combination of two things. One is that the pressure transducer tended to give pressure readings that were too high. This was observed when the transducer readings for the atmospheric pressure were compared to the readings taken from the barometer in the laboratory, which is considered the more accurate of the two. The transducer consistently gave higher readings than the barometer, by approximately 1%. The other possible reason for the offset in the curve is the fact that the atmospheric pressure used to calculate the Δp^2 values was taken from the barometer, not from the pressure transducer. Therefore in each of the Δp^2 terms, the pressure value for the inside of the pipe was too high and the external pressure value was fairly accurate thus making the Δp^2 values higher than they actually were. As was stated in Chapter II, the offset was corrected for by subtracting the amount of the offset from each of the Δp^2 readings. The constants obtained using the additional calibration data yielded values for the constants A and B that improved the results in the low mass flux region. Upon examining the range of mass fluxes in the

simulated heat pipe, it was found that most of the mass flux values were below 0.05 lbf-sec/ft^3. Another curve-fit was then made of only the calibration data up to 0.05 lbf-sec/ft^3, which produced values for A and B that further improved the results in the low mass flux region. Since the walls of the pipe used in these experiments were approximately half as thick as those used in Bowman's experiments, the value of B was expected to be less than the value that Bowman calculated. As it turned out, this value was about one fourth that of Bowman's.

The pressure distributions obtained from the tests with the simulated heat pipe showed a fluctuation in the pressure distribution in the condenser section rather than a smooth increase of pressure from the beginning to the end of the condenser. Kinney and Sparrow (6) noted that in the presence of wall suction, the change in momentum of the flow tended to increase the pressure in the flow direction, while the wall shear stress tended to decrease the pressure. In the first half of the condenser, the change in momentum was very small due to the small amount of suction through the walls and was approximately the same order of magnitude as the wall shear stress. Therefore the momentum change was not the dominant effect in this region and consequently the pressure did not exhibit a smooth increase.

Due to the compressible nature of the flow and the low design pressure drop across the pipe walls, the mass injection and removal along the pipe studied was non-uniform. As

was discussed previously, the mass flux through the pipe wall is dependent on the pressure difference across the pipe wall. Since the external pressure was relatively constant and the internal pressure varied axially along the pipe, the mass injection and removal also varied. The thinness of the pipe walls made the pressure drop across the pipe low, thus presenting less resistance to the mass flux. The pipe's internal pressure consequently remained quite close to the external pressure for a large portion of both the condenser and the evaporator sections. The pressure dropped off sharply in the last six inches of the evaporator, where most of the mass addition occurred, and rose sharply in the last half of the condenser, where most of the mass was removed. This suggests that there may be an optimum length or L/D for the pipe.

Numerical Results Discussion

In all of the numerical simulations, the flow in the evaporator section was assumed to be laminar throughout. This was a reasonable assumption since Bowman showed that the flow remains laminar, when injection is present, up to very large axial Reynolds numbers (on the order of 10^6). The values of the friction coefficients obtained from the numerical simulations were somewhat higher than the values predicted by Bowman's expression. In the evaporator section, where mass injection was present, Kinney's (5) results indicate that for laminar, incompressible flow with large injection wall Reynolds numbers, the product f^*Re_w should approach approximately 20.

For the incompressible region of the evaporator used in this study, the calculated friction coefficients are approximately one order of magnitude greater than Kinney's results. Bowman's laminar flow friction coefficient expression included the effect of the compressibility of the flow and thus extended Kinney's results for higher Mach numbers. Again the calculated friction coefficients are approximately one order of magnitude greater than the values predicted by Bowman's expression. Kinney's and Bowman's results indicate that the product f*Re remains essentially constant (approximately 20) for low Mach numbers and Bowman's expressions predict an increase as the Mach number increases toward 1 and greater. The results from this research were found to exhibit this trend for the f^*Re_∞ product versus Mach number, which can be seen in Figure 3.5, only the increase with Mach number begins at lower Mach numbers than Bowman's results.

The flow in the condenser section was assumed to be turbulent throughout in all of the numerical simulations. Bowman showed that once the flow entered the condenser, where an adverse pressure gradient was present, it transitioned to turbulent. He also found that the transition always started at the beginning of the condenser near the pipe wall, when the flow was subsonic, and then spread toward the center of the pipe as the flow progressed through the condenser. The location in the condenser where the turbulence reached the pipe center moved downstream as the axial velocity increased. Since the transition regions for the axial velocities attained

at the entrance to the condenser in this research were quite small relative to the overall condenser length, neglecting the transition region and assuming turbulent flow throughout was a reasonable assumption. The values computed for the friction coefficients in the condenser section were lower, by approximately one order of magnitude, than the values predicted by Bowman's turbulent flow friction coefficient expression. Bowman's expression indicated an increase in the f^*Re_∞ product with increased Mach number. When the results from the numerical simulation of the condenser were plotted as f^*Re_∞ versus Ma, the trend predicted by Bowman's expression was not seen as prominently as the trend shown in the evaporator, but it was present (see Figure 3.6).

There were several sources of error in the experimental study which could account for the difference between the calculated and expected results. As was mentioned earlier, there was a problem with the pressure transducer in the Scanivalve tending to read the pressures higher than what they actually were. This problem primarily affected the calibration results by giving a higher pressure differential for a given mass flux, which thus introduced error into the computed values of the constants A and B in Equation (2.1). Also there were no pressure taps in the last six inches of the evaporator section, preceding the condenser, where the pressure showed a sharper drop. Therefore, the accuracy of the interpolated pressures in that region is questionable. In all the numerical simulations, the friction coefficients near the end

of the evaporator were negative indicating that the change in momentum across the increment was greater than the change in pressure. This meant that the calibration equation (Equation (2.1)) was giving mass flux values that were too high for the given pressure difference, thus indicating that the calibration constants, A and B, were inaccurate.

The checks made in the numerical simulation code to verify the accuracy of the calculations all indicated that the simulations were giving accurate results. The force balance check yielded quite small positive values in all of the simulations and the mass balance check yielded small negative values for the low supply mass flow rates and small positive values for the higher supply mass flow rates. In all of the simulations, the mass flow rate entering the condenser was found to be too high. To correct this, the equation used to calculate the mass flux through the wall (Equation (2.1)) was multiplied by a correction factor. This correction factor increased with higher supply mass flow rates and ranged from approximately 0.70 to 0.85. The addition of the correction factor also improved the force and mass balances.

V. Conclusions and Recommendations

This chapter discusses the conclusions made from the findings of this research. In addition, a brief list of recommendations for further research is presented.

Conclusions

The data obtained from this research exhibited the same basic trends predicted by previous research, however differing by approximately one order of magnitude. The change in momentum of the flow has much more influence on the pressure change along the pipe than the friction force. Therefore, even though the values of the friction coefficients calculated in this work were much greater than those predicted by Bowman's expressions, the actual difference in the pressure distributions resulting from Bowman's friction values and those measured in the experimental portion of this research may not be as significant. Another numerical simulation utilizing Bowman's friction coefficient expressions to solve for the axial pressure distribution would be needed in order to make the comparison. The friction coefficient calculations were also found to be quite sensitive to the values computed for the calibration constants, A and B. The difference in the friction coefficients calculated from this research and that of Bowman's dropped from two orders of magnitude to one order of magnitude between the second and final curve-fits of the calibration data. The analysis of the results from the nu-

merical simulations seems to indicate that the either the data obtained in the calibration tests is inaccurate or the equation used to curve-fit the data (Equation (2.1)) does not give an accurate enough representation of the calibration results. Whichever is the case, the inaccuracy of the calibration equation seems to be the primary source of the discrepency with the results from previous research.

Recommendations

Upon examining the procedures used in this study, several recommendations can be made for improvements to this experiment and possibilities for future research. One recommendation which would improve the readings obtained from the pressure transducer is to subtract the transducer's atmospheric pressure reading from each reading made by the transducer to get a gauge pressure. The atmospheric pressure taken from a barometer can then be added to these gauge pressures to get the absolute pressure. This would help eliminate the offset in the calibration curve, which was observed in this study. Some of the recommendations for future research include:

1) Perform experiments to measure the velocity gradients along the wall as well as the pressure distribution along the pipe. This would provide more accurate information for computing the shear stress at the wall and should give more accurate results for the friction coefficients.

2) Perform a one-dimensional numerical simulation which utilizes Bowman's friction coefficient expressions to solve

for the pressure distribution along a heat pipe. Then perform experiments to measure the pressure distribution in a simulated heat pipe operating under the same conditions to check the computed results.

Appendix A: Raw Experimental Data

This appendix contains the raw data obtained in the experimental portion if this research. Each file gives the mass flow rate entering the test section and 34 pressure measurements. Figure 2.1 shows the location of the pressure taps in the test section. In general, pressure measurements 1 and 2 were for the pressure above and below the orifice plate respectively, 3 for the pressure at the upstream end of the evaporator manifold, 4 and 5 for the downstream end of the evaporator manifold, 6 and 7 for the atmospheric pressure, 8 - 13 for inside the evaporator section of the porous pipe, and 14 - 34 for inside the condenser end of the porous pipe. Pressure taps 8 - 13 were approximately six inches apart, 13 and 14 eight inches apart, 14 - 34 two inches apart. Pressure tap 34 was located at the end of the condenser section of the porous pipe. The total length of the test section was 6.976 feet. The air supply temperature for all runs was 72 ^{o}F $\pm$ 5 ^{o}F.

Data File: D2209B

Supply Mass Flow Rate (lbm/sec) = 0.043651

PORT	PRESSURE(psia)	PORT	PRESSURE(psia)
1	114.4222	18	14.4009
2	114.3897	19	14.4229
3	15.9113	20	14.4306
4	15.8919	21	14.5212
5	15.8867	22	14.5186
6	14.2250	23	14.5302
7	14.2186	24	14.5341
8	15.7949	25	14.2302
9	15.7664	26	14.7397
10	15.7238	27	14.7526
11	15.6423	28	14.8147
12	15.4638	29	14.8406
13	15.1871	30	14.8949
14	14.4009	31	14.9220
15	14.3091	32	14.9388
16	14.3298	33	14.9647
17	14.3337	34	14.9634

Data File: D2209C

Supply Mass Flow Rate (lbm/sec) = 0.058069

PORT	PRESSURE(psia)	PORT	PRESSURE(psia)
1	114.3252	18	14.3970
2	114.2675	19	14.4229
3	16.9626	20	14.4113
4	16.9264	21	14.5431
5	16.9173	22	14.5108
6	14.2121	23	14.5509
7	14.2250	24	14.5121
8	16.8527	25	14.2289
9	16.8152	26	14.9117
10	16.7583	27	14.9634
11	16.6535	28	15.0824
12	16.4195	29	15.1302
13	15.9669	30	15.2492
14	14.4203	31	15.3048
15	14.3052	32	15.3643
16	14.2929	33	15.3733
17	14.2949	34	15.3772

Data File: D2209D

Supply Mass Flow Rate (lbm/sec) = 0.070994

PORT	PRESSURE(psia)	PORT	PRESSURE(psia)
1	114.1545	18	14.3983
2	114.0680	19	14.4113
3	18.1315	20	14.3673
4	18.0876	21	14.5522
5	18.0501	22	14.4746
6	14.2186	23	14.5108
7	14.2069	24	14.4164
8	18.0229	25	14.2250
9	17.9699	26	15.0203
10	17.9065	27	15.1082
11	17.7876	28	15.3061
12	17.5018	29	15.3798
13	16.8785	30	15.5854
14	14.4526	31	15.6785
15	14.2845	32	15.7742
16	14.2470	33	15.8130
17	14.2716	34	15.8130

Data File: D2209E

Supply Mass Flow Rate (lbm/sec) = 0.083142

PORT	PRESSURE(psia)	PORT	PRESSURE(psia)
1	114.0550	18	14.4190
2	114.9359	19	14.4074
3	19.3833	20	14.3492
4	19.3096	21	14.5936
5	19.2721	22	14.4345
6	14.2186	23	14.4669
7	14.2147	24	14.2949
8	19.2773	25	14.2263
9	19.2216	26	15.0707
10	19.1466	27	15.2182
11	19.0186	28	15.4910
12	18.6915	29	15.6164
13	17.9324	30	15.8906
14	14.4875	31	16.0302
15	14.2936	32	16.1970
16	14.2225	33	16.2436
17	14.2612	34	16.2578

Data File: D2209G

Supply Mass Flow Rate (lbm/sec) = 0.108925

PORT	PRESSURE(psia)	PORT	PRESSURE(psia)
1	113.5972	18	14.4656
2	113.3916	19	14.4436
3	22.6264	20	14.3156
4	22.5579	21	14.6789
5	22.5605	22	14.3854
6	14.2225	23	14.3789
7	14.2108	24	13.9716
8	22.5346	25	14.2186
9	22.4777	26	15.1044
10	22.3950	27	15.3358
11	22.2462	28	15.8001
12	21.8583	29	16.1091
13	20.8510	30	16.6121
14	14.6169	31	16.9509
15	14.2897	32	17.3117
16	14.1487	33	17.4643
17	14.2095	34	17.5160

Data File: D2209H

Supply Mass Flow Rate (lbm/sec) = 0.12559

PORT	PRESSURE(psia)	PORT	PRESSURE(psia)
1	113.4084	18	14.4979
2	113.1343	19	14.4591
3	24.8079	20	14.3039
4	24.8661	21	14.7591
5	24.8726	22	14.3725
6	14.2056	23	14.3363
7	14.1992	24	13.8009
8	24.7187	25	14.2212
9	24.6424	26	15.0578
10	24.5558	27	15.3229
11	24.4161	28	15.9268
12	24.0359	29	16.4001
13	22.9484	30	17.0932
14	14.7268	31	17.5677
15	14.2781	32	18.0604
16	14.0893	33	18.2543
17	14.1888	34	18.2751

Data File: D2209I

Supply Mass Flow Rate (lbm/sec) = 0.13969

PORT	PRESSURE(psia)	PORT	PRESSURE(psia)
1	113.5312	18	14.5431
2	113.1923	19	14.4707
3	27.2235	20	14.2987
4	27.2597	21	14.8638
5	27.2700	22	14.3556
6	14.2082	23	14.3143
7	14.1992	24	13.6199
8	27.1446	25	14.2045
9	27.0683	26	14.9944
10	26.9726	27	15.2582
11	26.8135	28	15.9863
12	26.4256	29	16.5953
13	25.2256	30	17.5199
14	14.8716	31	18.1574
15	14.2677	32	18.8027
16	14.0169	33	19.0613
17	14.1733	34	19.1001

Data File: D2209J

Supply Mass Flow Rate (lbm/sec) = 0.15997

PORT	PRESSURE(psia)	PORT	PRESSURE(psia)
1	113.9075	18	14.5962
2	113.4640	19	14.4966
3	30.5765	20	14.2587
4	30.4433	21	14.9893
5	30.4562	22	14.3738
6	14.2056	23	14.2923
7	14.1953	24	13.4156
8	30.5274	25	14.2108
9	30.4343	26	14.9104
10	30.3140	27	15.0927
11	30.1343	28	15.9410
12	29.6778	29	16.7725
13	28.3161	30	18.0514
14	15.1613	31	18.9436
15	14.2755	32	19.8462
16	13.9315	33	20.1967
17	14.1552	34	20.2561

Data File: D0810A

Supply Mass Flow Rate (lbm/sec) = 0.19033

PORT	PRESSURE(psia)	PORT	PRESSURE(psia)
1	114.8473	18	14.9023
2	114.2306	19	14.7652
3	35.9310	20	14.4859
4	35.5198	21	15.4467
5	35.5172	22	14.5002
6	14.4174	23	14.4717
7	14.4161	24	13.3545
8	35.8961	25	14.4161
9	35.7939	26	15.0717
10	35.6491	27	14.9838
11	35.4564	28	15.8605
12	34.9469	29	17.0062
13	33.3719	30	18.8877
14	15.9291	31	20.2571
15	14.5118	32	21.6433
16	13.9752	33	22.2304
17	14.3527	34	22.4102

Data File: D0810B

Supply Mass Flow Rate (lbm/sec) = 0.238907

PORT	PRESSURE(psia)	PORT	PRESSURE (psia)
1	114.4594	18	15.3601
2	113.4785	19	15.0859
3	45.1444	20	14.9398
4	44.6841	21	15.9252
5	44.7410	22	14.7226
6	14.4122	23	14.5726
7	14.4135	24	13.0014
8	45.1302	25	14.3941
9	45.0035	26	15.2269
10	44.8289	27	14.7368
11	44.6026	28	14.9489
12	44.0492	29	16.3299
13	42.2272	30	19.9067
14	17.4950	31	22.4270
15	14.7769	32	24.8878
16	13.8859	33	25.8886
17	14.6902	34	26.1330

Appendix B: Sample Calculations

This appendix includes samples calculations for the pipe calibration and for the first step of the numerical simulation code.

Pipe Calibration Calculations

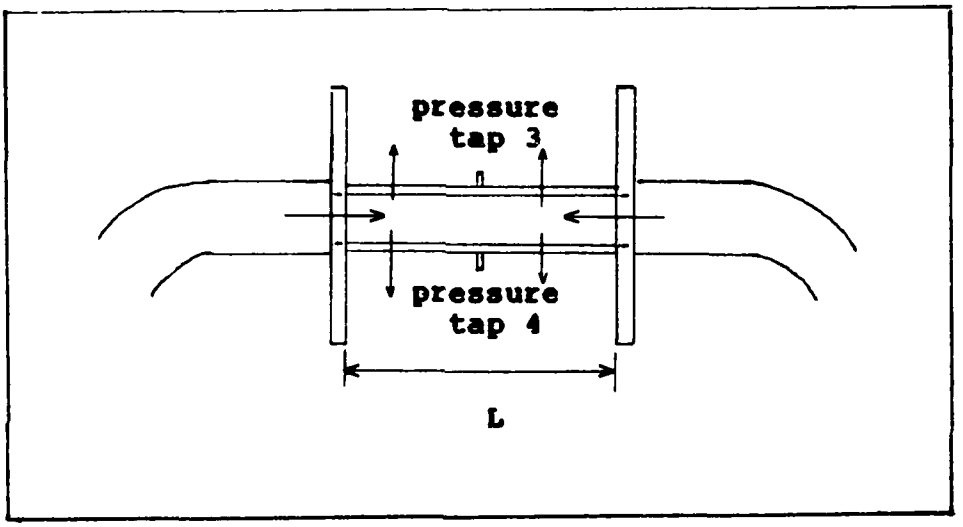

Figure B.1 Calibration Manifold

Pressure Tap 1 - Pressure upstream of the orifice plate, or pressure upstream of flowmeter, p_1

Pressure Tap 2 - Pressure downstream of orifice plate, p_2

Q = Mass flow rate

q = Flowmeter mass flow rate reading

A = surface area of the porous pipe

D = porous pipe diameter = 0.625 inches

D_1 = Air Supply Pipe Diameter = 3.062 inches

D_2 = orifice plate bore = 1.0 inch

L = length of porous pipe sample

k = 1.4

C = discharge coefficient = 0.61

$\beta = D_2/D_1 = 0.326584$

R = ideal gas constant for air = 53.26 lbf-ft/lbm-°R

$X = (p_1 - p_2)/p_1$

$Y = 1 - (0.41 + 0.35\,\beta^4)X/k$

Sample Readings from Orifice Plate Measurement of Mass Flow Rate:

$p_1 = 114.7224$ psia

$p_2 = 114.7007$ psia

$p_3 = 25.19472$ psia

$p_4 = 25.16627$ psia

$p_{atm} = 14.3558$ psia

T = 538 °R

L = 1.953 inches

X = 0.000189

Y = 0.99994

$\rho = p_1/(RT) = 0.5765$ lbm/ft³

Q = D_2 C Y [2 $(p_1 - p_2)/((1 - \beta^4)]^{1/2}/4$

Q = 0.03604 lbm/sec

$A = \pi D L = 0.02663$ ft²

$\rho v = Q/(Ag_c) = 0.04206$ lbf-sec/ft³

$\Delta p^2 = [(p_3 + p_4)/2]^2 - p_{atm}^2$

$\Delta p^2 = 8{,}874{,}344.45$ lbf²/ft⁴

Sample Readings from Flowmeter Mass Flow Rate Measurement:

p_1 = 15.00665 psia

p_3 = 14.68725 psia

p_4 = 14.68466 psia

p_{atm} = 14.37227 psia

q = 0.3975 cfm

T = 534 °R

L = 1.875 inches

$\rho = p_1/(RT) = 0.07598$ lbm/ft³

$Q = q\rho = 0.0005034$ lbm/sec

$A = \pi D L = 0.025566$ ft²

$\rho v = Q/(Ag_c) = 0.000612$ lbf-sec/ft³

$\Delta p^2 = [(p_3 + p_4)/2]^2 - p_{atm}^2 = 189{,}011.3$ lbf²/ft⁴

<u>Sample Calculations for First Increment of Numerical Simulation Code (x = 0.0 to x = 0.005 ft):</u>

(The data for these sample calculations is taken from the raw pressure data file D2209E)

p_u = pressure at the upstream end of the evaporator air supply manifold

p_u = 2791.20 lbf/ft²

p_d = pressure at the downstream end of the evaporator air supply manifold

p_d = 2777.88 lbf/ft²

p_1 = internal pressure at the upstream end of the evaporator

p_1 = 2781.648 lbf/ft²

p_2 = pressure at the first pressure tap location in the evaporator

$p_2 = 2775.931$ lbf/ft^2

p_3 = pressure at the second pressure tap location in the evaporator

$p_3 = 2767.910$ lbf/ft^2

$k = 1.4$

$D = 0.625$ in $= 0.0521$ ft

PL = total pipe length $= 6.976$ ft

A = constant from equation 2.1 $= 4.679 \times 10^9$ ft^2/sec^2

B = constant from equation 2.1 $= 4.2843 \times 10^7$ lbf/ft-sec

$T = 533.1$ °R

$x = 0.005$ ft

$x_1 = 0.00$ ft

x_2 = axial location of first pressure tap in the evaporator

$x_2 = 0.50$ ft

x_3 = axial location of second pressure tap in the evaporator

$x_3 = 0.99$ ft

Assuming the pressure in the evaporator changes linearly from upstream value to its downstream value, calculate the slope of the line.

$$S = (p_3 - p_u)/(PL/2) = -3.8188 \text{ lbf/ft}^3$$

$\rho_1 = p_1/(RT) = 0.0978$ lbm/ft^3

$A_{cs} = \pi D^2/4 = 0.002132$ ft^2

$A_{cv} = \pi D \Delta x = 0.0008184$ ft^2

$(\Delta p^2)_1 = p_1^2 - p_u^2 = -53{,}251.844$ lbf^2/ft^4 (negative sign

indicates mass flow into pipe)

$K_1 = [(x - x_2)(x - x_3)]/[(x_1 - x_2)(x_1 - x_3)] = 0.985$

$K_2 = [(x - x_1)(x - x_3)]/[(x_2 - x_1)(x_2 - x_3)] = 0.0201$

$K_3 = [(x - x_1)(x - x_2)]/[(x_3 - x_1)(x_3 - x_2)] = -0.0051$

$p(x = 0.005) = K_1p_1 + K_2p_2 + K_3p_3 = 2781.6048 \text{ lbf/ft}^2$

$p_m = p(x = 0.005)$

$p_{2'} = p_m + \delta x = 2791.18 \text{ lbf/ft}^2$

$(\Delta p^2)_2 = p_m^2 - p_{2'}^2 = -53{,}365.587 \text{ lbf}^2/\text{ft}^4$

$(\rho v) = -g_c[-B + (B^2 + 4A\,|(\Delta p^2)|)^{1/2}]/(2A)$ (from eqn 2.1)

$(\rho v)_1 = -0.035672 \text{ lbm/ft}^2\text{-sec}$

$(\rho v)_2 = -0.035740 \text{ lbm/ft}^2\text{-sec}$

$Ma_1 = 0.0$

u = axial velocity

$u_1 = 0.0$

$a^2 = g_c k p_1/\rho_1 = 1{,}281{,}139.47 \text{ ft}^2/\text{sec}^2$

$a = 1{,}131.87 \text{ ft/sec}$

$\dot{m}_1 = 0.0 \text{ lbm/sec}$

$(\rho v)_{avg} = [(\rho v)_1 + (\rho v)_2]/2 = -0.035706 \text{ lbm/ft}^2\text{-sec}$

$\rho_2 = p_2/(RT) = 0.0978 \text{ lbm/ft}^3$

$\rho_{avg} = (\rho_1 + \rho_2)/2 = 0.0978 \text{ lbm/ft}^3$

$u_2 = -(\rho v)_{avg} A_p/(\rho_{avg} A_m) = 0.14015 \text{ ft/sec}$

$Ma_2 = u_2/a = 0.0001238$

$u_{avg} = (u_1 + u_2)/2 = 0.07008 \text{ ft/sec}$

$Ma_{avg} = (Ma_1 + Ma_2)/2 = 0.0000619$

$\dot{m} = -(\rho v)_{avg} A_p = 0.0000292 \text{ lbm/sec}$

$\dot{m}_2 = \dot{m}_1 + \Delta\dot{m} = 0.0000292 \text{ lbm/sec}$

$\dot{m}_{avg} = (\dot{m}_1 + \dot{m}_2)/2 = 0.0000146 \text{ lbm/sec}$

$$\mu = 2.27(10^{-8})\ T^{3/2}/(T + 198.6) = 3.82(10^{-7})\ \text{lbf-sec/ft}^2$$

$$M = \text{momentum} = \dot{m}\ u$$

$$\Delta M = \dot{m}_2 u_2/g_c - \dot{m}_1 u_1/g_c = 1.2720 \times 10^{-7}\ \text{lbf}$$

$$\tau_w = [(p_1 - p_w)A_w - \Delta M\ ]/A_p = 0.11238\ \text{lbf/ft}^2$$

$$f = 2\ \tau_w\ g_c/(\rho_{ave} u_{ave}^2) = 15{,}056.123$$

$$Re_w = 4\ \dot{m}_{ave}/(\pi D \mu g_c) = 29.031$$

$$Re_w = (\ v)_{ave}\ D\ /(\mu g_c) = -151.360$$

Appendix C: Numerical Simulation Code and Sample Results

The following pages are a listing of the computer code used for the numerical simulations. The code is written in FORTRAN 77 and some sample results are also included following the program listing.

```
**************************************************************
*                                                            *
*      ONE-DIMENSIONAL HEAT PIPE SIMULATION PROGRAM          *
*                                                            *
**************************************************************
```

This program uses one-dimensional incompressible and compressible flow models to solve for the flow properties and friction coefficients in a closed porous pipe with blowing and suction. An incompressible model consisting of Newton's second law and incompressible flow equations is used to calculate flow properties until the Mach number reaches 0.01. After that, the compressible model, consisting of the continuity equation and Shapiro's method of influence coefficients, is used to solve for the properties.

DEFINITION OF VARIABLES:

A	Constant used in wall boundary condition (ft^2/sec^2)
AC	Cross-sectional area of the pipe (ft^2)
AP	Surface area of DX increment (ft^2)
B	Constant used in wall boundary condition (lbf/ft/sec)
C2	Speed of sound squared (ft^2/sec^2)
D	Pipe inside diameter (ft)
DMOM	Change in momentum across DX increment (lbf)
DX	Spacial step size (ft)
DW	Change in mass flow rate due to mass transfer at the wall (lbm/sec)
F	Friction factor
FS	Shear force over the increment DX (lbf)
FSSUM	Summation of all the incremental shear force values over the entire pipe (lbf)
FUD	Constant to account for the statistical variation of the porous pipe properties
GAM	Ratio of specific heats
GC	Constant in Newton's second law ($lbm-ft/lbf/sec^2$)
M1	Mach number at upstream end of DX increment
M2	Mach number at downstream end of DX increment
M12	M1 squared
M22	M2 squared
MSBAR	Average of M12 and M22
PATM	Atmospheric pressure (entered in psia then converted lbf/ft^2)
PCOND	Condenser environment pressure (lbf/ft^2)
PEVAPD	Downstream evaporator environment pressure (entered in psia then converted to lbf/ft^2)
PEVAPU	Upstream evaporator environment pressure (entered in psia then converted to lbf/ft^2)
PEX	Environment pressure (lbf/ft^2)
PL	Pipe length (ft)
P0	Upstream end of porous pipe pressure (lbf/ft^2)
P1	Static pressure at upstream end of DX increment (lbf/ft^2)

```
P2      Static pressure at downstream end of DX increment
        (lbf/ft²)
R       Ideal gas constant for air (lbf-ft/lbm/°R)
REW     Radial Reynolds number
REX     Axial Reynolds number
RHO     Density (lbm/ft³)
RHOV1   Mass flux through the wall at the upstream end of the
        DX increment (lbm/ft²/sec)
RHOV2   Mass flux through the wall at the downstream end of the
        DX increment (lbm/ft²/sec)
RMU     Viscosity (lbf-sec/ft²)
S       Slope of the evaporator environment pressure line
        (lbf/ft²/ft)
TW      Wall shear stress (lbf/ft²)
T0      Total air temperature (°R)
W1      Mass flow rate at the upstream end of the DX increment
        (lbm/sec)
W2      Mass flow rate at the downstream end of the DX incre-
        ment (lbm/sec)
XL      Local axial position (ft)
XND     Nondimensional axial location (XL/PL)
X(1)-X(30) Axial location of pressure measurements (ft)


DIMENSION X(30),P(30)
REAL K1,K2,K3,M1,M2,M12,M22,MSBAR
X(1) = 0.00
X(2) = 6.0/12.
X(3) = 11.9/12.
X(4) = 18./12.
X(5) = 23.9/12.
X(6) = 30./12.
X(7) = 35.9/12.
X(8) = 3.44633
X(9) = 3.52967
X(10) = 43.84/12.
X(11) = 45.78/12.
X(12) = 47.72/12.
X(13) = 49.72/12.
X(14) = 51.72/12.
X(15) = 53.66/12.
X(16) = 55.66/12.
X(17) = 57.72/12.
X(18) = 59.72/12.
X(19) = 61.69/12.
X(20) = 63.72/12.
X(21) = 65.69/12.
X(22) = 67.66/12.
X(23) = 69.66/12.
X(24) = 71.66/12.
X(25) = 73.66/12.
X(26) = 75.63/12.
X(27) = 77.66/12.
```

```
      X(28) = 79.72/12.
      X(29) = 81.72/12.
      X(30) = 6.976
      OPEN(9,FILE='results')
      OPEN(10,FILE='data')
      OPEN(12,FILE='fdat')
      READ(10,20) PATM
   20 FORMAT(F7.4 )
      WRITE(9,30) PATM
   30 FORMAT(3X,'PATM = ',F7.4,1x,'psia')
      READ(10,40) T0
   40 FORMAT(F6.2)
      WRITE(9,50) T0
   50 FORMAT(3X,'T0 = ',F6.2,'=R')
      READ(10,60) PEVAPU
   60 FORMAT(F7.4)
      WRITE(9,70) PEVAPU
   70 FORMAT(3X,'PEVAPU = ',F7.4,1x,'psia')
      READ(10,80) PEVAPD
   80 FORMAT(F7.4)
      WRITE(9,90) PEVAPD
   90 FORMAT(3X,'PEVAPD = ',F7.4,1x,'psia,/)
      DO 110 I = 2,7
      READ(10,100) P(I)
  100 FORMAT(F7.4)
      P(I) = P(I)*144.
  110 CONTINUE
      DO 115 I = 10,30
      READ(10,112) P(I)
  112 FORMAT(F7.4)
      P(I) = P(I)*144
  115 CONTINUE
      WRITE(6,120)
  120 FORMAT(3X,'ENTER THE FUDGE FACTOR')
      READ(5,130) FUD
  130 FORMAT(F5.3)
      WRITE(9,140) FUD
  140 FORMAT(3X,'FUD = ',F5.3,/)
      PATM = PATM*144.
      PEVAPU = PEVAPU*144.
      PEVAPD = PEVAPD*144.
      PCOND = PATM
      R = 53.335
      GAM = 1.4
      GAM1 = (GAM - 1)/2
      D = 0.625/12
      PL = 6.976
      PLH = PL/2
      DX = 0.005
      GC = 32.174
      PI = 3.1415927
      A = 4679000000.0
      B = 42843100.0
```

```
      K = 1
      FSSUM = 0.0
      DWSUM = 0.0

      ASSUMING THE EVAPORATOR ENVIRONMENT PRESSURE CHANGES LINEARLY
      FROM ITS UPSTREAM VALUE TO ITS DOWNSTREAM VALUE, CALCULATE THE
      SLOPE OF THE LINE.

      S = (PEVAPD - PEVAPU)/PLH

      CALCULATE THE PRESSURE IN THE PIPE AT THE UPSTREAM END USING
      THE FIRST THREE MEASURED PRESSURE VALUES.

      X1 = X(2)
      X2 = X(3)
      X3 = X(4)
      XC1 = X2*X3/((X1 - X2)*(X1 - X3))
      XC2 = X1*X3/((X2 - X1)*(X2 - X3))
      XC3 = X1*X2/((X3 - X1)*(X3 - X2))
      P(1) = P(2)*XC1 + P(3)*XC2 + P(4)*XC3
      P0 = P(1)/144

      CALCULATE THE PRESSURE AROUND THE CONDENSER ENTRANCE.
      P(8) = P(X=(PLH-0.5/12)); P(9) = P(X=(PLH+0.5/12))

      X0 = X(9)
      X1 = X(10)
      X2 = X(11)
      X3 = X(12)
      XC1 = ((X0 - X2)*(X0 - X3))/((X1 - X2)*(X1 - X3))
      XC2 = ((X0 - X1)*(X0 - X3))/((X2 - X1)*(X2 - X3))
      XC3 = ((X0 - X1)*(X0 - X2))/((X3 - X1)*(X3 - X2))
      P(9) = P(10)*XC1 + P(11)*XC2 + P(12)*XC3
      P(8) = P(9)
      DO 160 J = 1,30
      PT = P(J)/144
      WRITE(9,150) J,PT
  150 FORMAT(3X,'P(',I2,') = ',F7.4,1X,'psia')
  160 CONTINUE
      WRITE(9,170)
  170 FORMAT(//,45X,'RADIAL',9X,'AXIAL',/,4X,'X/L',7X,'FRICTION',10X,
     &'MACH',8X,'REYNOLDS',6X,'REYNOLDS',/,15X,'FACTOR',10X,'NUMBER',
     &8X,'NUMBER',8X,'NUMBER',7X,'BETA',/)
      WRITE(12,180)
  180 FORMAT(12X,'CALCULATED',9X,'BOWMANS',/,4X,'X/L',7X,'FRICTION',
     &8X,'FRICTION',/,15x,'FACTOR',10X,'FACTOR')

      INITIALIZE VARIABLES AT THE UPSTREAM PIPE END

      XL = 0.0
      W2 = 0.0
      M22 = 0.0
      P2 = P(1)
```

```
      T = T0
      PEX = PEVAPU
      RHO2 = P(1)/(R*T0)
      AC = PI*D**2/4.
      AP = PI*D*DX
      I = 1
      N = 1
      C = ABS(P2**2 - PEX**2)
      RHOV2 = -FUD*GC*(-B + SQRT(B**2 + 4.*A*C))/(2.*A)
      C2 = GC*GAM*P2/RHO2
      XL = XL + DX

      BEGIN MARCHING DOWN PIPE

      INCOMPRESSIBLE MODEL (M < 0.01) CALCULATIONS

  200 N = N + 1
      IF(XL.LE.X(3)) I = 1
      IF(XL.GT.X(3).AND.XL.LE.X(4)) I = 2
      IF(XL.GT.X(I+2)) I = I + 1
      IF(XL.GE.X(9).AND.XL.LE.X(11)) I = 9
      IF(XL.LT.X(8)) PEX = S*XL + PEVAPU
      IF(XL.GT.X(9)) PEX = PCOND
      W1 = W2
      M12 = M22
      M1 = SQRT(M12)
      U1 = M1*SQRT(C2)
      P1 = P2
      RHOV1 = RHOV2
      RHO1 = RHO2
      IF(XL.GT.X(8).AND.XL.LT.X(9)) GO TO 210

      INTERPOLATE TO FIND THE PRESSURE AT STATION 2

      X1 = X(I)
      X2 = X(I+1)
      X3 = X(I+2)
      CC1 = P(I)/((X1 - X2)*(X1 - X3))
      CC2 = P(I+1)/((X2 - X1)*(X2 - X3))
      CC3 = P(I+2)/((X3 - X1)*(X3 - X2))
      P2 = CC1*(XL-X2)*(XL-X3)+CC2*(XL-X1)*(XL-X3)+CC3*(XL-X1)*(XL-X2)
      XND = XL/PL
      GO TO 220
  210 P2 = P(9)
      RHOV2 = 0.0
      XND = XL/PL
      GO TO 230

      CALCULATE THE PROPERTIES AT STATION 2

  220 C = P2**2 - PEX**2
      ID = 1
      IF(C.LT.0.0) ID = -1
```

```
      C = ABS(C)
      RHOV2 = ID*FUD*GC*(-B + SQRT(B**2 + 4*A*C))/(2*A)
  230 RHOVAV = (RHOV1 + RHOV2)/2
      RHO2 = P2/(R*T)
      RHOBAR = (RHO1 + RHO2)/2
      U2 = RHO1*U1/RHO2 - RHOVAV*AP/(RHO2*AC)
      M22 = U2**2/C2
      M2 = SQRT(M22)
      UBAR = (U1 + U2)/2
      MSBAR = (M12 + M22)/2
      CON1 = 1 + GAM1*MSBAR
      T = T0/CON1
      DW = -RHOVAV*AP
      DWSUM = DWSUM + DW
      IF(XL.GT.3.489.AND.XL.LT.3.491) WCK = DWSUM
      W2 = W1 + DW
      WBAR = (W1 + W2)/2
      RMU = 2.27E-08*SQRT(T**3)/(T + 198.6)
      REX = 4*WBAR/(PI*D*RMU*GC)
      REW = RHOVAV*D/(RMU*GC)
      BETA = ABS(REW/REX)
      DMOM = W2*U2/GC - W1*U1/GC
      TW = ((P1 - P2)*AC - DMOM)/AP
      FS = TW*AP
      FSSUM = FSSUM + FS
      F = 2*GC*TW/(RHOBAR*UBAR**2)
      AREX = ABS(REX)
      FSTAR = 0.046/AREX**0.2
      IF(XL.LE.3.488) THEN
         FB = 16/REX*1.2337*EXP(1.2*MSBAR)
      ELSE
         FB = FSTAR*(1+55*AREX**.1*EXP(1.2*MSBAR)*BETA**.9*PL/D**.1)
      END IF
      CK = N/20 - K
      IF(N.LT.10) GO TO 260
      IF(CK.EQ.0.0) GO TO 260
  250 XL = XL + DX
      IF(XL.GT.PL) GO TO 390

      CHECK TO SEE IF THE MACH NUMBER HAS REACHED 0.01.  IF IT HAS,
      SWITCH TO COMPRESSIBLE FLOW CALCULATIONS.

      IF(M2.LE.0.01) GO TO 200
      GO TO 300

  260 WRITE(9,270) XND,F,M2,REW,REX,BETA
  270 FORMAT(3X,F5.3,3X,F14.7,5X,F9.7,4X,F10.3,4X,F9.2,4X,F7.4)
      WRITE(12,282) XND,F,FB
  282 FORMAT(3X,F5.3,3X,F14.7,4X,F7.4)
      IF(N.LT.10) GO TO 290
      K = K + 1
  290 GO TO 250
```

```
      COMPRESSIBLE FLOW CALCULATIONS

  300 N = N + 1
      IF(XL.LE.X(3)) I = 1
      IF(XL.GT.X(3).AND.XL.LE.X(4)) I = 2
      IF(XL.GT.X(I+2)) I = I + 1
      IF(XL.GE.X(9).AND.XL.LE.X(11)) I = 9
      IF(XL.LT.X(8)) PEX = S*XL + PEVAPU
      IF(XL.GT.X(9)) PEX = PCOND
      W1 = W2
      P1 = P2
      RHO1 = RHO2
      RHOV1 = RHOV2
      C2 = GC*GAM*P1/RHO1
      M12 = M22
      M1 = SQRT(M12)
      U1 + M1*SQRT(C2)
      IF(XL.GT.X(8).AND.XL.LT.X(9)) GO TO 310

      INTERPOLATE TO FIND THE PRESSURE AT STATION 2

      X1 = X(I)
      X2 = X(I+1)
      X3 = X(I+2)
      PP1 = P(I)
      PP2 = P(I+1)
      PP3 = P(I+2)
      K1 = PP1/((X1 - X2)*(X1 - X3))
      K2 = PP2/((X2 - X1)*(X2 - X3))
      K3 = PP3/((X3 - X1)*(X3 - X2))
      P2 = K1*(XL-X2)*(XL-X3)+K2*(XL-X1)*(XL-X3)+K3*(XL-X1)*(XL-X2)
      XND = XL/PL
      GO TO 320
  310 P2 = P(9)
      RHOV2 = 0.0
      XND = XL/PL
      GO TO 330

      CALCULATE THE PROPERTIES AT STATION 2

  320 C = P2**2 - PEX**2
      ID = 1
      IF(C.LT.0.0) ID = -1
      C = ABS(C)
      RHOV2 = ID*FUD*GC*(-B + SQRT(B**2 + 4*A*C))/(2*A)
  320 RHOVAV = (RHOV1 + RHOV2)/2
      RHO2 = P2/(R*T)
      RHOBAR = (RHO1 + RHO2)/2
      DW = -RHOVAV*AP
      DWSUM = DWSUM + DW
      IF(XL.GT.3.489.AND.XL.LT.3.491) WCK = DWSUM
      W2 = W1 + DW
      WBAR = (W1 + W2)/2
```

```
      CM = M12*(1 + GAM1*M12)*((W2/W1)**2)/((P2/P1)**2)
      M22 = (-1 + SQRT(1 + 4*GAM1*CM))/(2*GAM1)
      M2 = SQRT(M22)
      MSBAR = (M12 + M22)/2
      CON1 = 1 + GAM1*MSBAR
      T = T0/CON1
      C2 = GC*GAM*P2/RHO2
      U2 = M2*SQRT(C2)
      UBAR = (U1 + U2)/2
      CFP = (1 + GAM*MSBAR)/(GAM*MSBAR)
      F = 0.5*(D/DX)*(ALOG(M12/M22) - CFP*ALOG(P2/P1))
      TW = 0.5*F*RHOBAR*UBAR**2/GC
      FS = TW*AP
      FSSUM = FSSUM + FS
      RMU = 2.27E-08*SQRT(T**3)/(T + 198.6)
      REX = 4*WBAR/(PI*D*RMU*GC)
      AREX = ABS(REX)
      REW = RHOVAV*D/(RMU*GC)
      BETA = ABS(REW/REX)
      FSTAR = 0.046/AREX**0.2
      IF(XL.LE.3.488) THEN
         FB = 16/REX*1.2337*EXP(1.2*MSBAR)
      ELSE
         FB = FSTAR*(1+55*AREX**.1*EXP(1.2*MSBAR)*BETA**.9*PL/D**.1)
      END IF
      CK = N/20 - K
      IF(CK.EQ.0.0) GO TO 360
350   XL = XL + DX

      CHECK TO SEE IF THE MACH NUMBER IS LESS THAN 0.01.  IF IT IS,
      SWITCH BACK TO THE INCOMPRESSIBLE FLOW CALCULATIONS.

      IF(M2.LE.0.01) GO TO 200
      IF(XL.LE.PL) GO TO 300
      GO TO 390

360   WRITE(9,370) XND,F,M2,REW,REX,BETA
370   FORMAT(3X,F5.3,3X,F14.7,5X,F9.7,4X,F10.3,4X,F9.2,4X,F7.4)
      WRITE(12,382) XND,F,FB
382   FORMAT(3X,F5.3,3X,F14.7,4X,F10.8)
      K = K + 1
      GO TO 350

390   WRITE(9,400) XND,F,M2,REW,REX,BETA
400   FORMAT(3X,F5.3,3X,F14.7,5X,F9.7,4X,F10.3,4X,F9.2,4X,F7.4)
      WRITE(12,402) XND,F,FB
402   FORMAT(3X,F5.3,3X,F14.7,4X,F10.8)

      COMPUTE THE FORCE BALANCE FOR THE ENTIRE TUBE.

      TEST = (P(1) - P(30))*AC - FSSUM
      WRITE(9,410) TEST,DWSUM
410   FORMAT(///,3X,'FORCE BALANCE =',F10.6,1X,'lbf',/,3X,'MASS BAL
```

```
     &ANCE =',F6.4,1x,'lbm/sec')
      WRITE(9,430) WCK
  430 FORMAT(3X,'Mass Flow Rate Entering Condenser = ',F9.6,2X,'lbm
     &/sec')
      CLOSE(9)
      CLOSE(10)
      CLOSE(12)
      STOP
      END
```

TEST RUN #1

Supply Mass Flow Rate = 0.043651 lbm/sec

X/L	FRICTION FACTOR	MACH NUMBER	RADIAL REYNOLDS NUMBER	AXIAL REYNOLDS NUMBER	BETA
0.100	0.099048	0.018950	-152.061	7338.27	0.0207
0.200	0.009700	0.043203	-200.811	16726.01	0.0120
0.286	0.014217	0.071810	-283.298	27673.49	0.0102
0.372	0.002657	0.116745	-454.632	44442.84	0.0102
0.458	0.002902	0.191619	-735.807	71123.53	0.0103
0.515	0.036181	0.238237	252.702	86213.31	0.0029
0.630	0.007313	0.214018	210.720	76998.80	0.0027
0.716	0.016780	0.180273	297.061	65117.74	0.0046
0.816	0.000037	0.137835	496.930	50632.88	0.0098
0.917	0.049359	0.061729	566.242	18444.70	0.0311

Force Balance = 0.000287 lbf
Mass Balance = -0.0017 lbm/sec
Mass Flow Rate Entering Condenser = 0.043609 lbm/sec

TEST RUN #2

Supply Mass Flow Rate = 0.05807 lbm/sec

X/L	FRICTION FACTOR	MACH NUMBER	RADIAL REYNOLDS NUMBER	AXIAL REYNOLDS NUMBER	BETA
0.100	0.141391	0.018950	-166.655	7813.22	0.0213
0.200	0.015890	0.045054	-238.355	18550.60	0.0128
0.286	0.012252	0.078081	-355.141	31957.85	0.0111
0.372	0.004333	0.132968	-602.620	53589.23	0.0112
0.458	0.009795	0.237445	-1116.898	91363.22	0.0122
0.515	0.024286	0.317003	304.803	115901.25	0.0026
0.630	0.006685	0.293726	236.765	106504.06	0.0022
0.716	0.012464	0.256543	322.585	93158.14	0.0035
0.816	0.007668	0.202693	680.665	75699.05	0.0090
0.917	0.052697	0.093339	847.757	35334.37	0.0240

Force Balance = 0.000401 lbf
Mass Balance = -0.0021 lbm/sec
Mass Flow Rate Entering Condenser = 0.058174 lbm/sec

TEST RUN #3

Supply Mass Flow Rate = 0.08314 lbm/sec

X/L	FRICTION FACTOR	MACH NUMBER	RADIAL REYNOLDS NUMBER	AXIAL REYNOLDS NUMBER	BETA
0.100	0.257199	0.017478	-191.912	8233.66	0.0233
0.200	0.018961	0.045229	-298.903	21284.82	0.0140
0.286	0.011061	0.082000	-456.309	38352.21	0.0119
0.372	0.007456	0.147045	-842.995	67432.07	0.0125
0.458	0.018558	0.295485	-1823.500	124460.97	0.0147
0.515	0.018951	0.444090	434.329	167551.89	0.0026
0.630	0.007233	0.425127	277.450	158030.16	0.0018
0.716	0.009127	0.389829	272.125	143841.27	0.0019
0.816	0.011444	0.331650	877.220	127711.84	0.0069
0.917	0.045913	0.172545	1303.856	68633.47	0.0190

Force Balance = 0.001650 lbf
Mass Balance = 0.0031 lbm/sec
Mass Flow Rate Entering Condenser = 0.082912 lbm/sec

TEST RUN #4

Supply Mass Flow Rate = 0.108925 lbm/sec

X/L	FRICTION FACTOR	MACH NUMBER	RADIAL REYNOLDS NUMBER	AXIAL REYNOLDS NUMBER	BETA
0.100	0.277404	0.015766	-209.028	8673.28	0.0241
0.200	0.020153	0.042822	-353.672	23576.27	0.0150
0.286	0.009342	0.081075	-567.222	44358.81	0.0128
0.372	0.007461	0.151141	-1077.390	81042.14	0.0133
0.458	0.030118	0.331755	-2603.963	157456.94	0.0165
0.515	0.017825	0.565882	629.444	223004.86	0.0028
0.630	0.006598	0.554932	350.555	213668.03	0.0016
0.716	0.006495	0.521664	219.242	197495.28	0.0011
0.816	0.011422	0.471743	957.041	187507.56	0.0051
0.917	0.033950	0.265377	1754.761	112193.95	0.0156

Force Balance = 0.024062 lbf
Mass Balance = 0.0122 lbm/sec
Mass Flow Rate Entering Condenser = 0.108535 lbm/sec

TEST RUN #5

Supply Mass Flow Rate = 0.139692 lbm/sec

X/L	FRICTION FACTOR	MACH NUMBER	RADIAL REYNOLDS NUMBER	AXIAL REYNOLDS NUMBER	BETA
0.100	0.480220	0.013170	-274.625	8659.52	0.0317
0.200	0.000749	0.044702	-500.176	29494.15	0.0170
0.372	0.000610	0.161377	-1314.178	104268.41	0.0126
0.458	0.041324	0.362343	-3468.318	200480.73	0.0173
0.515	0.017733	0.701334	942.027	294288.41	0.0032
0.630	0.006167	0.706376	439.304	284733.22	0.0015
0.716	0.004396	0.674508	185.863	264785.41	0.0007
0.816	0.009445	0.635675	896.208	260769.89	0.0034
0.917	0.027973	0.375817	2200.172	171322.94	0.0128

Force Balance = 0.123370 lbf
Mass Balance = 0.0289 lbm/sec
Mass Flow Rate Entering Condenser = 0.140039 lbm/sec

BIBLIOGRAPHY

1. Bean, H. S. Fluid Meters, Their Theory and Application (Sixth Edition). New York: The American Society of Mechanical Engineers, 1971.

2. Bowman, Capt William J. Heat Pipe Vapor Dynamics. PhD dissertation. School of Engineering, Air Force Institute of Technology (AU), Wright-Patterson AFB OH, June 1987 (88182592).

3. Chi, S. W. Heat Pipe Theory and Practice. New York: McGraw-Hill Book Company, 1976.

4. Dunn, P. and D. A. Reay. Heat Pipes (Second Edition). London: Perganon Press, 1978.

5. Kinney, R. B. "Fully Developed Frictional and Heat Transfer Characteristics of Laminar Flow in Porous Tubes," International Journal of Heat and Mass Transfer, 11: 1393-1401 (April 1968).

6. Kinney, R. B. and E. M. Sparrow. "Turbulent Flow, Heat Transfer, and Mass Transfer in a Tube with Surface Suction," Journal of Heat Transfer, 117-125 (February 1970).

7. Muskat, M. The Flow of Homogeneous Fluids Through Porous Media. Ann Arbor: J. W. Edwards, Inc., 1946.

8. Quaile, J. P. and E. K. Levy. "Laminar Flow in a Porous Tube with Suction," Journal of Heat Transfer, Transactions of the ASME, 66-71 (February 1975).

9. Shapiro, A. H. The Dynamics and Thermodynamics of Compressible Fluid Flow, Vol. 1. New York: The Ronald Press Company, 1953.

10. Wageman, W.E. and F. A. Guevara. "Fluid Flow Through a Porous Channel," The Physics of Fluids, 3 (6): 878-881 (Nov-Dec 1960).

11. Yuan, S. W. and A. B. Finkelstein. "Laminar Pipe Flow with Injection and Suction Through a Porous Wall," Journal of Heat Transfer, Transactions of the ASME: 719-724 (May 1956).

VITA

Second Lieutenant Constance A. Holladay was born on 23 March 1964 in Memphis, Tennessee. She attended Overton High School in Memphis, Tennessee and graduated in 1982. From September 1982 to May 1986, she attended Memphis State University where she studied Mechanical Engineering. Upon graduation, she received the degree of Bachelor of Science in Mechanical Engineering and a commission in the USAF through the ROTC program. Following graduation, she entered the School of Engineering, Air Force Institute of Technology, in May 1986.

Permanent address: 932 Inman Rd
Memphis, Tennessee 38111

UNCLASSIFIED
SECURITY CLASSIFICATION OF THIS PAGE

REPORT DOCUMENTATION PAGE

Form Approved
OMB No. 0704-0188

1a. REPORT SECURITY CLASSIFICATION UNCLASSIFIED	1b. RESTRICTIVE MARKINGS
2a. SECURITY CLASSIFICATION AUTHORITY	3. DISTRIBUTION/AVAILABILITY OF REPORT Approved for public release; distribution unlimited.
2b. DECLASSIFICATION/DOWNGRADING SCHEDULE	
4. PERFORMING ORGANIZATION REPORT NUMBER(S) AFIT/GAE/AA/87D-6	5. MONITORING ORGANIZATION REPORT NUMBER(S)
6a. NAME OF PERFORMING ORGANIZATION School of Engineering 6b. OFFICE SYMBOL (If applicable) AFIT/ENY	7a. NAME OF MONITORING ORGANIZATION
6c. ADDRESS (City, State, and ZIP Code) Air Force Institue of Technology (AU) Wright-Patterson AFB, Ohio 45433-6583	7b. ADDRESS (City, State, and ZIP Code)
8a. NAME OF FUNDING/SPONSORING ORGANIZATION Power Technology Group 8b. OFFICE SYMBOL (If applicable) AFWAL/POOC-5	9. PROCUREMENT INSTRUMENT IDENTIFICATION NUMBER
8c. ADDRESS (City, State, and ZIP Code) Power Technology Group AFWAL/POOC-5 Wright-Patterson AFB, Ohio 45433	10. SOURCE OF FUNDING NUMBERS PROGRAM ELEMENT NO. / PROJECT NO. / TASK NO / WORK UNIT ACCESSION NO.

11. TITLE (Include Security Classification)

COMPRESSIBLE FRICTION COEFFICIENTS IN A SIMULATED HEAT PIPE

12. PERSONAL AUTHOR(S)

Constance A. Holladay, 2d Lt, USAF

13a. TYPE OF REPORT	13b. TIME COVERED	14. DATE OF REPORT (Year, Month, Day)	15. PAGE COUNT
MS Thesis	FROM _____ TO _____	1987 December	79

16. SUPPLEMENTARY NOTATION

17. COSATI CODES			18. SUBJECT TERMS (Continue on reverse if necessary and identify by block number)
FIELD	GROUP	SUB-GROUP	
20	04		Heat Pipe, Fluid Dynamics, Mass Transfer, Internal Friction

19. ABSTRACT (Continue on reverse if necessary and identify by block number)

Thesis Advisor: James E. Hitchcock
Professor of Mechanical Engineering

Approved for public release IAW AFR 190-1.
LYNN E. WOLAVER
Dean for Research and Professional Development
Air Force Institute of Technology (AU)
Wright-Patterson AFB OH 45433

20. DISTRIBUTION/AVAILABILITY OF ABSTRACT	21. ABSTRACT SECURITY CLASSIFICATION
☒ UNCLASSIFIED/UNLIMITED ☐ SAME AS RPT. ☐ DTIC USERS	UNCLASSIFIED
22a. NAME OF RESPONSIBLE INDIVIDUAL James E. Hitchcock, Professor	22b. TELEPHONE (Include Area Code) (513) 255-3517
	22c. OFFICE SYMBOL AFIT/ENY

DD Form 1473, JUN 86 Previous editions are obsolete.

SECURITY CLASSIFICATION OF THIS PAGE
UNCLASSIFIED

19. Research was performed to verify previously obtained friction coefficients for compressible, laminar and turbulent flow in a simulated heat pipe for intermediate mass injection and suction rates. The research was divided into two main parts: an experimental study and a numerical study. In the experimental study, the axial pressure distribution along the simulated heat pipe, consisting of a long porous tube with air as the working fluid, was measured for various mass flow rates. The experimentally measured axial pressure distributions were then used as input to a one-dimensional numerical simulation to determine the friction coefficients. Finally, the results were compared to the previous research.

END
DATE
FILMD
3-88
DTIC